To the Graduate Council:

I am submitting herewith a thesis written by Byungsoo Kim entitled "*The Effect of Thermal Creep in an Enclosure Under Variable Gravity Conditions.*" I have examined the final copy of this thesis for form and content and recommend that it be accepted in partial fulfillment of the requirement for the degree of Master of Science, with major in Mechanical Engineering.

Majid Parang

Dr. M. Parang, Major Professor

We have read this thesis and recommend its acceptance:

Majid Keyhani

Dewald R. Pitts

Accepted for the Council:

Cwminkel

Associate Vice Chancellor
and Dean of The Graduate School

STATEMENT OF PERMISSION TO USE

In presenting this thesis in partial fulfillment of the requirement for a Master of Science degree at The University of Tennessee, Knoxville, I agree that the Library shall make it available to borrowers under rules of the Library. Brief quotations from this thesis are allowable without special permission, provided that accurate acknowledgment of the source is made.

Permission for extensive quotation from or reproduction of this thesis may be granted by my major professor, or in his absence, by the Head of Interlibrary Services when, in the opinion of either, the proposed use of the material is for scholarly purposes. Any copying or use of the material in this thesis for financial gain shall not be allowed without my written permission.

Signature [illegible]

Date Aug. 10, 1998

THE EFFECT OF THERMAL CREEP IN AN ENCLOSURE UNDER VARIABLE GRAVITY CONDITIONS

A Thesis

Presented for the

Master of Science

Degree

The University of Tennessee, Knoxville

Byungsoo Kim

December 1994

Copyright © 1994

by

Byungsoo Kim

and

Dr. Parang, M.

All rights reserved

ACKNOWLEDGEMENTS

I would like to thank my major professor Dr. M. Parang for providing guidance and motivation in completing my thesis. I appreciate the support and help provided to me by the members of my thesis committee: Dr. M. Keyhani, Dr. R. Pitts. I would also like to thank Dr. Rao V. Arimilli for his suggestions and advice. I am also thankful for the support and encouragement I received from my friends and family members. Finally, I thank God for allowing me to attempt and finish this work.

ABSTRACT

A thermophoretic phenomenon, known as "thermal creep," has recently become the focus of several studies in flow analysis under microgravity conditions. Thermal creep drives a slip flow from lower to higher temperature regimes over a wall nonuniform temperature. It is suggested that in microgravity environment where the effect of buoyancy is reduced, the effect of thermal creep may become important and even critical in the kinematics and heat transfer of enclosed fluids.

This study presents a numerical analysis of a vapor movement inside a rectangular enclosure under a variable gravity condition and in the presence of thermal creep. Three different thermal boundary conditions are considered; a linear wall temperature along sidewalls, a nonlinear wall temperature along sidewalls, and a linear wall temperature along sidewalls in conjunction with heating from below. The results are obtained by solving the governing equations for velocity and temperature fields. A control volume formulation and SIMPLER algorithm are used in the numerical investigation of the problem.

It is found that under microgravity conditions, thermal creep induced by a nonisothermal wall would significantly alter the behavior of flow, but heat transfer remains dominated by conduction. As the gravity (buoyancy) effects increase, the resulting flow patterns are observed to be more complicated than pure buoyancy-induced flow. At certain critical values of gravity vector, the buoyancy effects and thermal creep are observed to achieve parity. Under these conditions, the flow is unstable and convective heat transfer become important. For large values of gravity, the effect of thermal creep is observed to be limited to the layers near the walls with nonuniform temperatures.

In general, the results indicate that thermal creep can be very important under microgravity condition and its effects should be included in applications in which the movement of a gas over a surface with nonuniform temperature is of interest.

TABLE OF CONTENTS

TABLE OF CONTENTS
(continued)

Page

LIST OF TABLES

LIST OF FIGURES

LIST OF FIGURES
(continued)

LIST OF SYMBOLS

a	Coefficient in the discretization equation
b	Constant term in the discretization equation
c_s	Coefficient of thermal slip
D	Diffusion conductance
F	Flow rate through a control-volume face
g	Gravitational acceleration
Gr	Grashof number, $Gr = g\beta(T_h - T_0)L^3/\nu^2$
H	Height of an enclosure
Kn	Knudsen number, $Kn = \lambda/L$
L	Width of an enclosure
N	Proportional constant
N_{CR}	Temperature change ratio, $N_{CR} = (T_h - T_c)/T_c$
Nu	Average Nusselt number (defined in Section 2.2)
P	Total pressure; also non-dimensional form of pressure
p'	Pressure deviation from initial(static) value
Pr	Prandtl number, $Pr=\nu/\alpha$
R	Universal gas constant
t	Time
T	Local absolute temperature
W	Width of an enclosure
u, v	Velocity component in x and y direction
U, V	Non-dimensional form of velocity components, u and v
x, y	Cartesian coordinates
X, Y	Non-dimensional Cartesian coordinates

Greek

α	Thermal diffusivity
β	Volume expansion coefficient
ϕ	General dependent variable

LIST OF SYMBOLS
(continued)

Γ	General diffusion coefficient
λ	Mean free path
μ	Dynamic viscosity
ν	Kinematic viscosity
θ	Non-dimensional temperature
τ	Non-dimensional time
ρ	Density
τ	Non-dimensional time

Subscripts

b	Evaluated value on the bottom wall
c	Value on the cold surface
E	Neighbor on the east side
e	Control-volume face between P and E
h	Value on the hot surface
l	Evaluated value on the left wall
N	Neighbor on the north side
n	Control-volume face between P and N
nb	General neighbor grid point
P	Central grid point under consideration
S	Neighbor on the south side
s	Control-volume face between P and E
t	Evaluated value on the top wall
W	Neighbor on the west side
w	Evaluated value on particular wall; also control-volume face between P and E
x	Component in x direction
y	Component in y direction
∞	Value at the location far from an object
0	Initial value

LIST OF SYMBOLS
(continued)

Superscripts

^	Pseudo velocity
*	A guessed pressure; also velocities based on the guessed pressure
'	Correction term

Abbreviations

PVT	Physical vapor transport
AR	Aspect ratio of the enclosure, $AR = H/L$

Chapter 1
INTRODUCTION

It is known that a wall with a nonzero surface temperature gradient in contact with a fluid, generates a slip flow over the wall surface. This phenomenon, called "thermal creep," is often neglected in most earth-bound flows due to the overwhelming dominance of forces associated with gravity. However, thermal creep can attain importance and may have to be included in the analysis of fluid and heat transfer processes in microgravity environment when buoyancy effects are not significant.

The fundamental physical process in thermal creep was first investigated by Maxwell to explain the radiometric force at low pressure[1]. Thermal creep exists due to unequal tangential momentum of molecules coming from the hot and the cold side as they impinge on the wall. This is sketched in Figure 1.1. To compensate for the uneven momentum transfer, a wall shear stress is generated which drives the fluid from the cold to the hot region over the wall surface. The resulting creep velocity, v_c for an ideal gas is proportional to the wall temperature gradient by[2]

$$v_c = \frac{c_s \mu R}{P} \frac{\partial T}{\partial y} \tag{1.1}$$

where c_s is the coefficient of thermal slip and is an order one term, and μ, R, P, and y are the dynamic viscosity, gas constant, the local pressure, and the distance along the wall, respectively. It should be noted that although the study of this phenomenon was originally motivated by application in rarefied flow regime, thermal creep is present and may become the important in continuum regime. The coefficient of thermal slip c_s,was first calculated by Maxwell to be 3/4. However, a more accurate value that is in substantial agreement with other kinetic theory analyses and is valid for wide range of Knudsen numbers (the

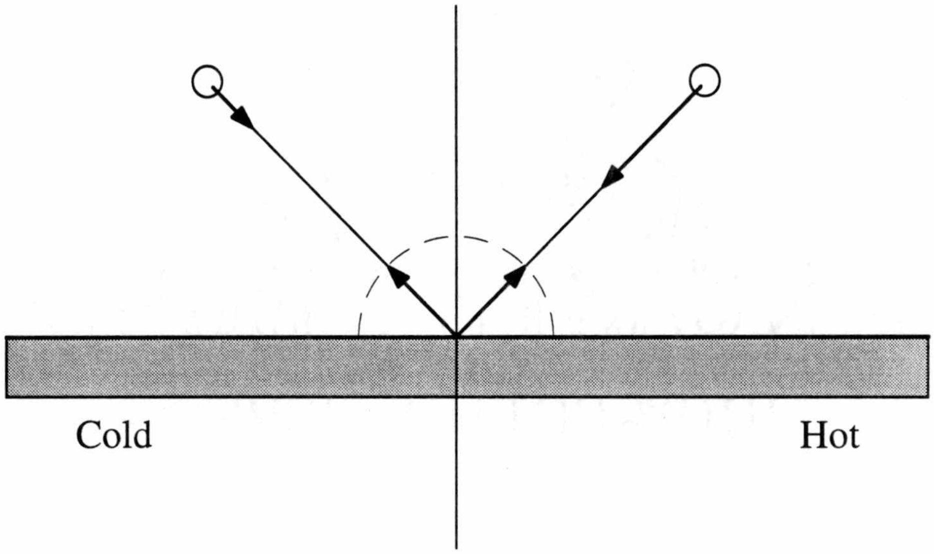

Figure 1.1 Schematic illustrating the basic of thermal creep

ratio of the molecular mean free path to the characteristic dimension of the problem) is 1.17[4]. This value will be also used in this study.

One of the applications in which creep flow analysis may prove significant is the formation of crystals by physical vapor transport (PVT) under microgravity conditions. In general, PVT is an important technique to grow crystals in closed ampoules by subliming materials below their melting points at one end of the enclosure and, after transport through a vapor space, recondensing them in single crystalline form. In the absence of motion induced by buoyancy in a low gravity condition, it is expected that a more uniform growth and enhanced crystal homogeneity are achieved[3]. However, in the presence of significant motion induced by thermal creep the flow pattern within a PVT vapor space, and the subsequent formation of crystals, may be affected. Therefore, a careful analysis of thermal creep in space environment may prove to be very important.

Rosner and Keyes[5,6] have pointed out that under typical microgravity conditions several neglected gas kinetic phenomena become important sources of convection in PVT. Among these phenomena, thermal creep may have a strong influence on the flow kinematics in the space microgravity condition. They estimated that even in *ground-based experiments* with ampoules at typical PVT pressures, induced sidewall creep velocity could be within an order of magnitude of those associated with conventional buoyancy-induced vapor velocity. For example, in an ampoule used to grow copper phthalocyanine films and with typical set of parameters g=980 cm/sec^2, p=3.2 Torr, ν=73 cm^2/sec, and temperature difference of 330K over a sidewall length of L=7.5 cm, thermal creep velocity is nearly 5 cm/sec which is about 7% of expected buoyancy-induced velocity.

Vedha-Nayagm and Mackowski[8] supported this observation by analyzing flow on a vertical wall with nonuniform temperature. Assuming steady, laminar flow, and a constant-property fluid and using Boussinesq and boundary-layer approximations, they found that a similarity solution exists when the surface temperature of the wall varies as $T_w = T_\infty + Ny^3$, where T_∞ is the temperature of the quiescent ambient fluid far away from the wall, N is a positive constant, and y is the distance along the wall. The important parameters were the Prandtl number Pr and Gr/Re^2, where the Gr is local Grashof number and *Re* is local Reynolds number based on the thermal creep velocity. The problem was solved for values of Gr/Re^2 between 0 and 100, and a fixed value of the Prandtl number of 0.7. Thermal creep effects were significant for values of Gr/Re^2 less than approximately 20, and buoyancy effects was dominant for values of Gr/Re^2 less than 1. For Gr/Re^2 around 25 and at one atmosphere pressure, the resulting mass flow rate and heat transfer rate were 25% greater than that computed by a pure buoyancy-induced convection. They concluded that thermal creep can significantly alter flow and heat transfer characteristics when buoyancy is negligible.

A numerical analysis of physical vapor transport in cylindrical ampoules under zero gravity conditions, including thermal creep boundary condition, was conducted by Walker, Nackowski, and Knight[8]. Different aspect ratios, temperature ratios, and Schmidt numbers (ratio of diffusion of momentum to diffusion of mass) were considered at the zero gravity condition. They found that for Schmidt numbers greater than ten, temperature ratio greater than 0.9 and smaller aspect ratio than 5.0, the thermal creep boundary condition significantly influenced the flux of the material from the source to the crystal.

Walker, Nackowski, and Knight did not include the effect of small gravity (g-jitter) and only considered flow induced by thermal creep. In microgravity space conditions, the effective gravity level within the space vehicle can be as large as 10^{-4}g due to various factors including crew movement, operation of equipment and vehicle maneuvers. For this reason inclusion of small gravity and the analysis of relative importance between creep-induced and buoyancy-induced motion are very important in a thorough understanding of flow kinetics in space environment.

In the present study, the importance of thermal creep in a rectangular enclosure containing an ideal gas is investigated by examining the kinematics of the flow and heat transfer. The analysis includes numerical solution of the mass, momentum, and energy conservation equations. An enclosure with different thermal boundary conditions is considered including one similar to a PVT ampoule. The investigation includes the examination of the relative importance of thermal creep to buoyancy-induced flow in space environments at various gravitational strengths.

Chapter 2
NUMERICAL ANALYSIS

2.1 Scope of Analysis

The focus of this study is on an ideal gas enclosed by a two-dimensional cavity of width L and height H as shown in Figure 2.1. The fluid is subjected to an arbitrary low gravity environment and various different thermal boundary conditions. These boundary conditions include:

(1) a linear wall temperature along sidewalls, with other walls insulated,

(2) a nonlinear wall temperature along sidewalls, with other walls insulated, and

(3) a linear wall temperature along the sidewalls in conjunction with isothermal (heated) bottom and (cold) top walls.

The magnitude of the gravitational vector ranges from zero to levels expected in typical microgravity applications. Various wall temperature gradients and aspect ratios are also considered. The dimensionless parameters of the problem are determined based on realistic geometry and temperature conditions. The gravitational vector is selected with parallel or normal components relative to the sidewall.

Under the assumptions of unsteady, two-dimensional, ideal gas with constant properties and the Boussinesq approximation, mass, momentum and energy conservation equations are solved numerically. Heat transfer is treated by calculating the average Nusselt number for each wall. The developed finite difference code is based on Patankar's control volume method[9] for the solution of a general differential equation containing unsteady, diffusion, and source terms, and it includes a staggered node arrangement for velocity computation and a power law scheme for the coefficients of discretized equations. The SIMPLER algorithm[9] is used to solve the discretized equations.

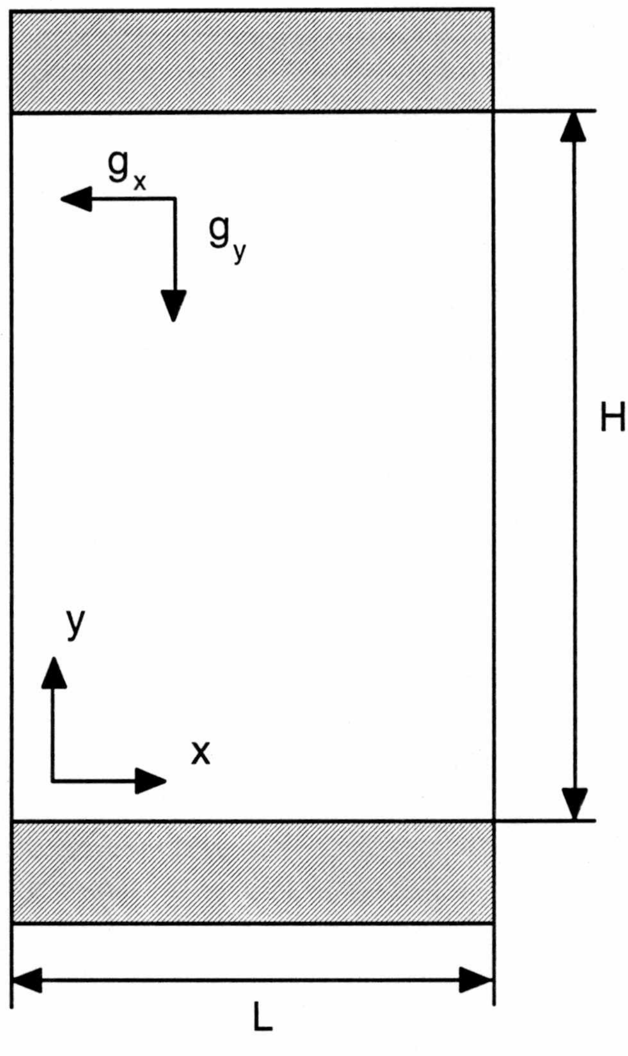

Figure 2.1 The enclosure considered in this study

2.2 Governing Equations

The dimensional governing equations for the unsteady, two-dimensional flow of a constant-property fluid with the Boussinesq approximation are

Mass:

$$\frac{\partial u}{\partial x}+\frac{\partial v}{\partial y}=0 \tag{2.1}$$

Newton's Second Law:

$$\begin{aligned}
\frac{\partial u}{\partial t}+u\frac{\partial u}{\partial x}+v\frac{\partial u}{\partial y}&=-\frac{1}{\rho}\frac{\partial p'}{\partial x}+\nu\left(\frac{\partial^2 u}{\partial x^2}+\frac{\partial^2 u}{\partial y^2}\right)+g_x\beta(T-T_0)\\
\frac{\partial v}{\partial t}+u\frac{\partial v}{\partial x}+v\frac{\partial v}{\partial y}&=-\frac{1}{\rho}\frac{\partial p'}{\partial y}+\nu\left(\frac{\partial^2 v}{\partial x^2}+\frac{\partial^2 v}{\partial y^2}\right)+g_y\beta(T-T_0)
\end{aligned} \tag{2.2}$$

Conservation of Energy:

$$\frac{\partial T}{\partial t}+u\frac{\partial T}{\partial x}+v\frac{\partial T}{\partial y}=\alpha\left(\frac{\partial^2 T}{\partial x^2}+\frac{\partial^2 T}{\partial y^2}\right) \tag{2.3}$$

where $\alpha=\frac{k}{\rho c_p}$, $p'=P-\rho(g_x x+g_y y)$, $\mathbf{g}=-g_x\mathbf{i}-g_y\mathbf{j}$ and (u, v), P, p′, T, and T_0 are velocity components in (x, y) coordinates, local pressure, pressure deviation from the hydrostatic value, fluid temperature, and initial fluid temperature, respectively. Also ν, α, β, and g are kinematic viscosity, thermal diffusivity, volume expansion coefficient, and gravitational acceleration, respectively.

To normalize the equations, the spatial lengths x and y are scaled by the enclosure width L. Since all length scales are normalized by the same reference length, aspect ratio effects appear through the boundary conditions. The velocities are scaled by viscous penetration velocity ν/L. This proves to be numerically convenient when a wide range of gravity values, from thermal-creep-dominant regimes to buoyancy-dominant regimes, is investigated. As a result, the normalized velocity is in effect local Reynolds number. Introducing the following normalized variables:

$$X = \frac{x}{L}, \quad Y = \frac{y}{L}, \quad U = \frac{uL}{\nu}, \quad V = \frac{vL}{\nu}$$

$$P = \frac{p'L^2}{\rho\nu^2}, \quad \theta = \frac{T - T_0}{T_h - T_0}, \quad \tau = \frac{t\nu}{L^2}$$

the governing equations become:

$$\frac{\partial U}{\partial X} + \frac{\partial V}{\partial Y} = 0 \tag{2.4}$$

$$\begin{aligned} \frac{\partial U}{\partial \tau} + U\frac{\partial U}{\partial X} + V\frac{\partial U}{\partial Y} &= -\frac{\partial P}{\partial X} + \frac{\partial^2 U}{\partial X^2} + \frac{\partial^2 U}{\partial Y^2} + Gr_x\theta \\ \frac{\partial V}{\partial \tau} + U\frac{\partial V}{\partial X} + V\frac{\partial V}{\partial Y} &= -\frac{\partial P}{\partial Y} + \frac{\partial^2 V}{\partial X^2} + \frac{\partial^2 V}{\partial Y^2} + Gr_y\theta \end{aligned} \tag{2.5}$$

$$\frac{\partial \theta}{\partial \tau} + U\frac{\partial \theta}{\partial x} + V\frac{\partial \theta}{\partial y} = \frac{1}{Pr}\left(\frac{\partial^2 \theta}{\partial X^2} + \frac{\partial^2 \theta}{\partial Y^2}\right) \tag{2.6}$$

where $Pr = \frac{\nu}{\alpha}$, $Gr_x = \frac{g_x\beta(T_h - T_0)L^3}{\nu^2}$, and $Gr_y = \frac{g_y\beta(T_h - T_0)L^3}{\nu^2}$

The heat transfer from the walls to the enclosed fluid is investigated by defining Nusselt number based on the integrated normal temperature gradient along each wall as follows:

Left sidewall

$$Nu_l = AR\int_0^{AR} -\left.\frac{\partial \theta}{\partial X}\right|_{X=0} dY$$

Bottom wall

$$Nu_b = AR\int_0^1 -\left.\frac{\partial\theta}{\partial Y}\right|_{Y=0} dX$$

where aspect ratio AR is the ratio of the height to the width of the cavity. Nusselt number at the other walls can be defined similarly .

2.3 Boundary Conditions

The schematic of the geometry of the problem is shown in Figure 2.1. The gravity vector is assumed to be aligned in the negative y-direction unless otherwise indicated. The height of the enclosure is H, and the width of the domain, which is selected as a characteristic length, is L. In the symmetric cases, the actual width of the enclosure is twice the width of the calculation domain. Boundary conditions are specified at each wall, i.e., for x=0, x=L, y=0 and y=H (or in normalized form, X=0, X=1, Y=0 and Y=AR where AR is the ratio of H to L.)

2.3.1 Linear Wall Temperature (Case I)

The first case considered in this study is shown in Figure 2.2. The left vertical wall is heated and is subjected to a linear wall temperature. The right vertical wall is subjected to a symmetric temperature boundary condition. The two horizontal walls are assumed to be insulated. The symmetrical nature of the boundary conditions imposed makes it convenient to consider only the left half of the enclosure as shown in Figure 2.2. The plane of symmetry is now assumed as an adiabatic surface with zero velocity gradient. These boundary conditions can be summarized as

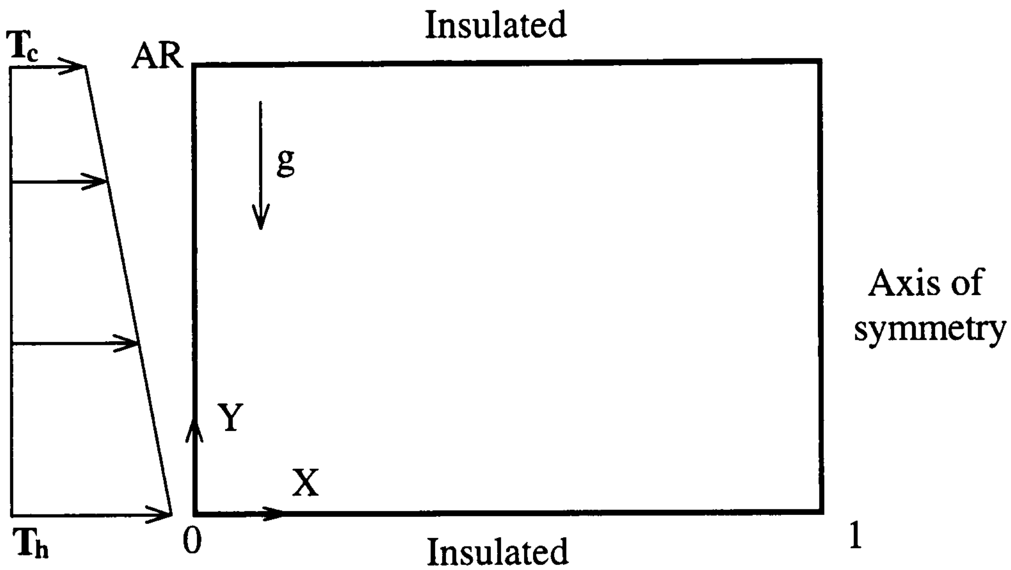

$$T_w = T_h - \frac{T_h - T_c}{H} y$$

Boundary Conditions

At Y=0 and Y=AR: $\quad U = 0, \quad V = 0, \quad \dfrac{\partial \theta}{\partial Y} = 0,$

At X=1: $\quad U = 0, \quad \dfrac{\partial V}{\partial X} = 0, \quad \dfrac{\partial \theta}{\partial X} = 0,$

At X=0: $\quad U = 0, \quad V = \dfrac{c_s N_{CR}}{AR(N_{CR}\theta + 1)}, \quad \theta = 1 - \dfrac{Y}{AR},$

where $AR = \dfrac{H}{L}, \quad N_{CR} = \dfrac{T_h - T_c}{T_c}$

At τ=0: $\quad U = 0, \quad V = 0, \quad \theta = 0$

Figure 2.2 The problem and boundary conditions of Case I at Y=0 and Y=AR: $\quad U=0, \quad V=0, \text{ and } \dfrac{\partial\theta}{\partial Y}=0,$

at X=1: $\quad U=0, \quad \dfrac{\partial V}{\partial X}=0, \text{ and } \dfrac{\partial\theta}{\partial X}=0,$

at X=0: $\quad U=0, \quad V=\dfrac{c_s L}{T_w}\left(-\dfrac{T_h-T_c}{H}\right)=\dfrac{c_s N_{CR}}{AR(N_{CR}\theta+1)},$

$$\text{and } \theta=1-\frac{Y}{AR}$$

where $AR=\dfrac{H}{L}$, and $N_{CR}=\dfrac{T_h-T_c}{T_c}$

N_{CR} is designated the creep number, and it represents the relative temperature change along the wall compared to the cold temperature responsible for driving the thermal creep flow.

2.3.2 *Nonlinear Wall Temperature (Case II)*

Another and more complex set of boundary conditions employed in this investigation is depicted in Figure 2.3. The temperature along the left vertical wall decreases nonlinearly as a function of y. The chosen nonlinear temperature distribution is a third order polynomial in y. The temperature along the right vertical wall also increases nonlinearly as a cubic power of y. Therefore, imposed thermal creep flow on the left wall is exactly the same set but opposite to that on the right wall. The two horizontal walls are assumed to be insulated. The boundary conditions can therefore be summarized as:

at Y=0 and Y=AR: $\quad U=0, \quad V=0, \text{ and } \dfrac{\partial\theta}{\partial Y}=0,$

at X=0: $\quad U=0, \quad V=\dfrac{c_s L}{T_w}\left(-3N(H-y)^2\right)=-\dfrac{3c_s N_{CR}(1-Y/AR)^2}{AR(N_{CR}\theta_w+1)},$

$$\text{and } \theta_w=\left(1-\frac{Y}{AR}\right)^3,$$

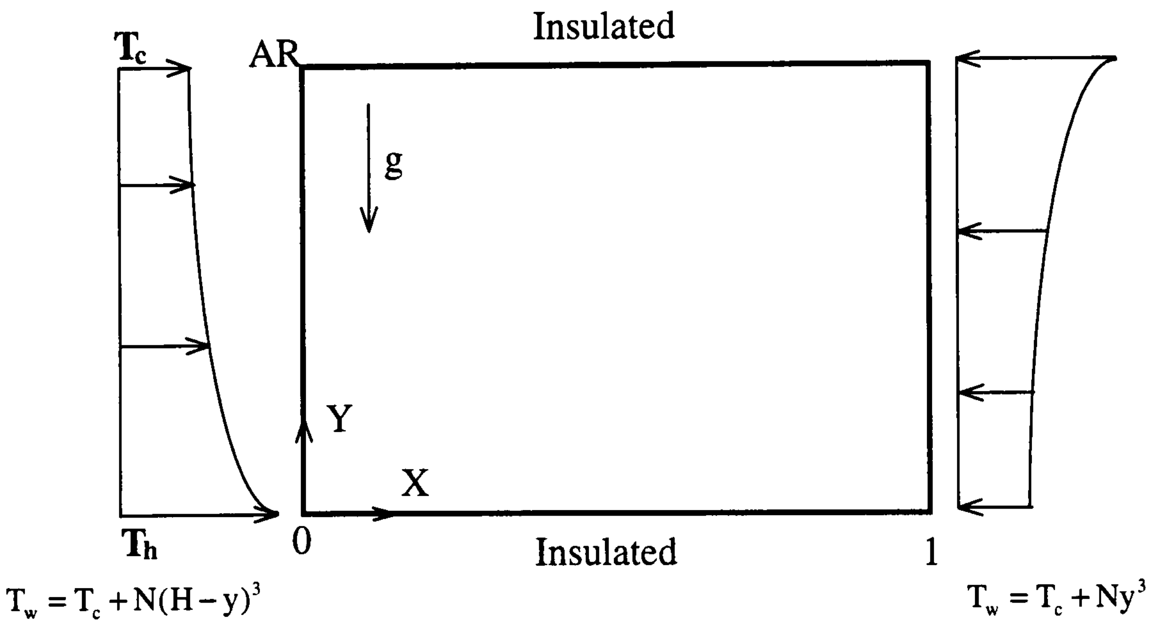

Boundary Conditions

At Y=0 and Y=AR: $\quad U=0, \quad V=0, \quad \dfrac{\partial\theta}{\partial Y}= \quad ,$

At X=0: $\quad U=0, \quad V=-\dfrac{3c_s N_{CR}(1-Y/AR)^2}{AR(N_{CR}\theta_w+1)}, \quad \theta_w=\left(1-\dfrac{Y}{AR}\right)^3,$

At X=1: $\quad U=0, \quad V=\dfrac{3c_s N_{CR} Y^2}{AR^3(N_{CR}\theta_w+1)}, \quad \theta_w=\left(\dfrac{Y}{AR}\right)^3$

Figure 2.3 The problem and boundary conditions of Case II at X=1: $U=0, \quad V=\frac{c_s L}{T_w}\left(3Ny^2\right)=\frac{3c_s N_{CR} Y^2}{AR^3\left(N_{CR}\theta_w+1\right)},$

$$\text{and } \theta_w=\left(\frac{Y}{AR}\right)^3$$

2.3.3 Linear Sidewall Temperature Distribution with Isothermal Horizontal Walls (Case III)

The third case considered is shown in Figure 2.4. The top and bottom walls are isothermal. The vertical sidewall temperature varies linearly from the top to the bottom horizontal wall temperatures. This case resembles the thermal boundary conditions imposed on physical vapor transport (PVT) ampoules both in normal and microgravity conditions. The only difference compared to a PVT application is the absence of mass transfer on the top and bottom walls. The boundary conditions are

at Y=0: $U=0, \quad V=0, \text{ and } \theta=1$

at Y=AR: $U=0, \quad V=0, \text{ and } \theta=0$

at X=1: $U=0, \quad \frac{\partial V}{\partial X}=0, \text{ and } \frac{\partial \theta}{\partial X}=0$

at X=0: $U=0, \quad V=\frac{c_s L}{T_w}\left(-\frac{T_h-T_c}{H}\right)=-\frac{c_s N_{CR}}{AR\left(N_{CR}\theta+1\right)},$

$$\text{and } \theta=1-\frac{Y}{AR}$$

2.3.4 Enclosures Subject to Multi-Component Gravity Vector (Case IV)

To investigate the effects of the orientation of the geometry in the boundary conditions of Case III, three different gravity vectors are considered: positive y-direction, negative x-direction and positive x-direction (see Figure 2.1). The calculation is done by

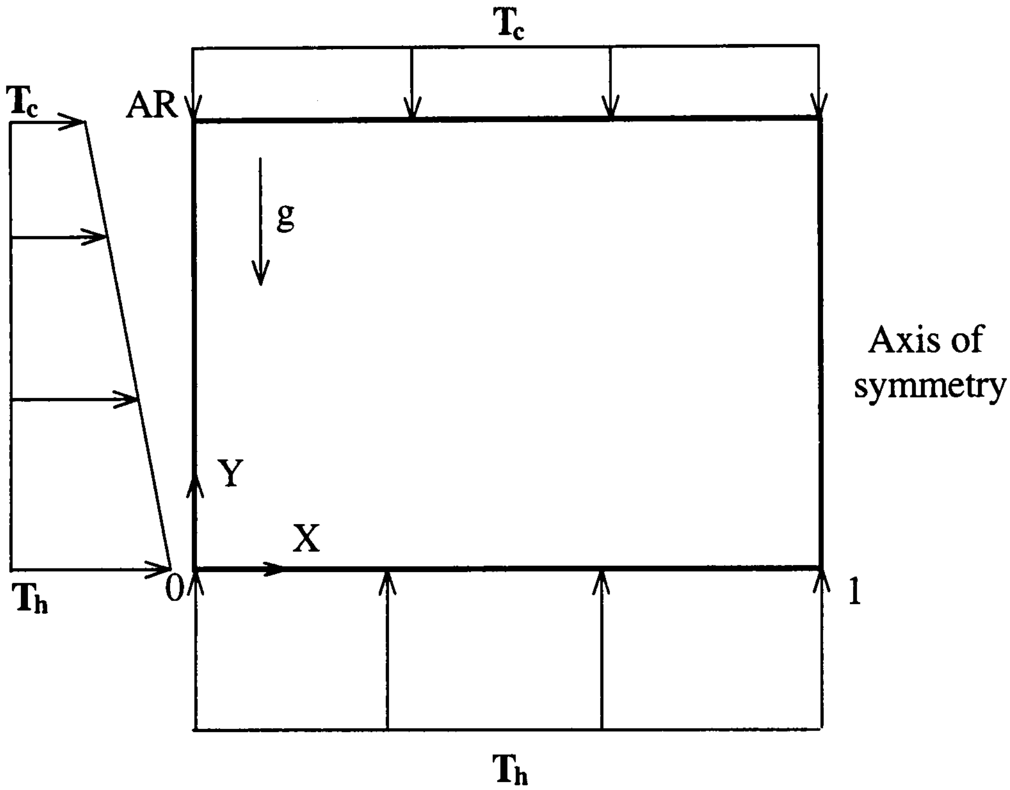

Boundary Conditions

At Y=0: $U = 0, \quad V = 0, \quad \theta = 1,$

At Y=AR: $U = 0, \quad V = 0, \quad \theta = 0,$

At X=1: $U = 0, \quad \dfrac{\partial V}{\partial X} = 0, \quad \dfrac{\partial \theta}{\partial X} = 0,$

At X=0: $U = 0, \quad V = -\dfrac{c_s N_{CR}}{AR(N_{CR}\theta + 1)}, \quad \theta = 1 - \dfrac{Y}{AR}$

Figure 2.4 The problem and boundary conditions of Case III substituting appropriate values in Gr_x and Gr_y into Equation (2.5). In Cases I through III where the gravity is in negative y-direction, Gr_x is zero and Gr_y is a positive constant. For these different gravity vectors, the following was used in Equation (2.5):

for positive y-direction gravity, $Gr_x = 0$, and $Gr_y = -375$

for negative x-direction gravity, $Gr_x = 375$, and $Gr_y = 0$

for positive x-direction gravity, $Gr_x = 375$, and $Gr_y = 0$.

2.4 Discretization of Equations

2.4.1. General governing differential equation

The governing equations discussed earlier can be cast in the form of a generalized conservation equation for a general dependent variable ϕ as:

$$\rho\frac{\partial\phi}{\partial t}+\rho u\frac{\partial\phi}{\partial x}+\rho v\frac{\partial\phi}{\partial y}=\Gamma\left(\frac{\partial^2\phi}{\partial x^2}+\frac{\partial^2\phi}{\partial y^2}\right)+S \tag{2.7}$$

where Γ is the diffusion coefficient, and S is the source term. The quantities Γ and S depend on a particular interpretation of ϕ. For example, if ϕ represents temperature, Γ and S become the ratio of the thermal conductivity to the specific heat (Γ) and volumetric source divided by the specific heat (S), respectively. As a consequence, all the governing differential equations discretized here, can be considered as particular cases of this general equation. Therefore, Equation (2.7) can be used for different meanings of ϕ, and appropriate interpretations for Γ and S, in a numerical scheme to provide the solution for velocity and temperature fields represented by the system of Equations (2.4)-(2.6).

2.4.2. Discretization

The numerical method is based on balancing appropriate terms from Equation (2.7) for a control volume. A typical control volume is illustrated in Figure 2.5. The specific details of the derivation of the discretization equation are given in Appendix A. The resulting discretization equation for variable ϕ in this control volume can be written as

$$a_P\phi_P = a_E\phi_E + a_W\phi_W + a_N\phi_N + a_S\phi_S + b \tag{2.8}$$

where

$$\begin{aligned}
a_E &= D_e A(|P_e|) + \max(-F_e, 0) \\
a_W &= D_w A(|P_w|) + \max(F_w, 0) \\
a_N &= D_n A(|P_n|) + \max(-F_n, 0) \\
a_s &= D_s A(|P_s|) + \max(F_s, 0) \\
a_P^o &= \frac{\rho^o \Delta x \Delta y}{\Delta t} \\
b &= S_c \Delta x \Delta y + a_P^o \phi_P^o
\end{aligned}$$

$$a_P = a_E + a_W + a_N + a_S + a_P^o - S_P \Delta x \Delta y$$

The corresponding conductance (D), the mass flow rates (F), and Peclet numbers (P) are defined by

$$\begin{aligned}
D_e &= \frac{\Gamma_e \Delta y}{\delta x_e}, & F_e &= (\rho u)_e \Delta y, & P_e &= \frac{F_e}{D_e} \\
D_w &= \frac{\Gamma_w \Delta y}{\delta x_w}, & F_w &= (\rho u)_w \Delta y, & P_w &= \frac{F_w}{D_w} \\
D_n &= \frac{\Gamma_n \Delta x}{\delta y_n}, & F_n &= (\rho v)_n \Delta x, & P_n &= \frac{F_n}{D_n} \\
D_s &= \frac{\Gamma_s \Delta x}{\delta y_s}, & F_s &= (\rho v)_s \Delta x, & P_s &= \frac{F_s}{D_s}
\end{aligned}$$

Several forms for the function A(|P|) can be selected. It is suggested that a power-law form for A(|P|) provides a good numerical accuracy at a relatively small CPU cost, when compared with other schemes [9]. For this reason a power-law is selected for the function A(|P|),

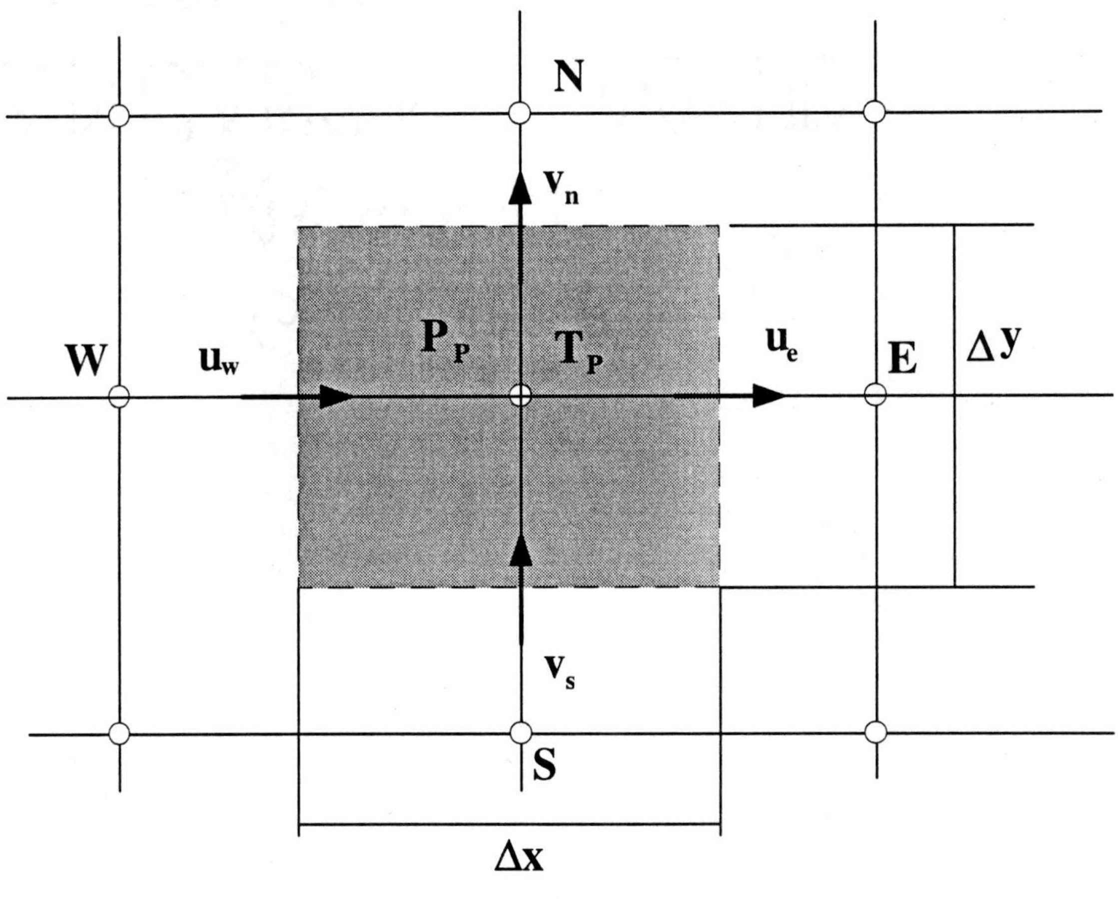

Figure 2.5 The control volume and definition of associated symbols

$$A(|P|) = [0, (1-0.1|P|)^5]$$

where the bracket [A,B] denotes the greater of A and B.

2.4.3. The Staggered Grid

To avoid numerical problems, a staggered grid is needed for the computation of velocity in the momentum equations. In the staggered grid, the velocity components are calculated at the middle of the faces of the control volume. Therefore, the x-direction component of velocity u is evaluated at the faces normal to the x-direction. The other velocity component v is evaluated at the middle of the horizontal sides of the control volume. Figure 2.6 shows a staggered control volume for Newton's Second Law in the x-direction. Since pressure is defined at the center of the main node, the resulting discretization equation can be written as

$$a_e u_e = \sum a_{nb} u_{nb} + b + (p_P - p_E)\Delta y \qquad (2.9)$$

The term b is defined in the same way as in the generalized discretization equation, but the pressure gradient is not included in the source-term quantities S_C and S_P.

Similarly, the discretization equation for the y-direction momentum equation can be shown to be

$$a_n v_n = \sum a_{nb} v_{nb} + b + (p_P - p_N)\Delta x \qquad (2.10)$$

2.4.4. The Pressure Correction Equation

The corrected pressure p can be calculated from

$$p = p^* + p'$$

where p* is the guessed pressure and p' is the pressure correction. In a similar manner, the velocity can be obtained from

$$u = u^* + u', \quad v = v^* + v'$$

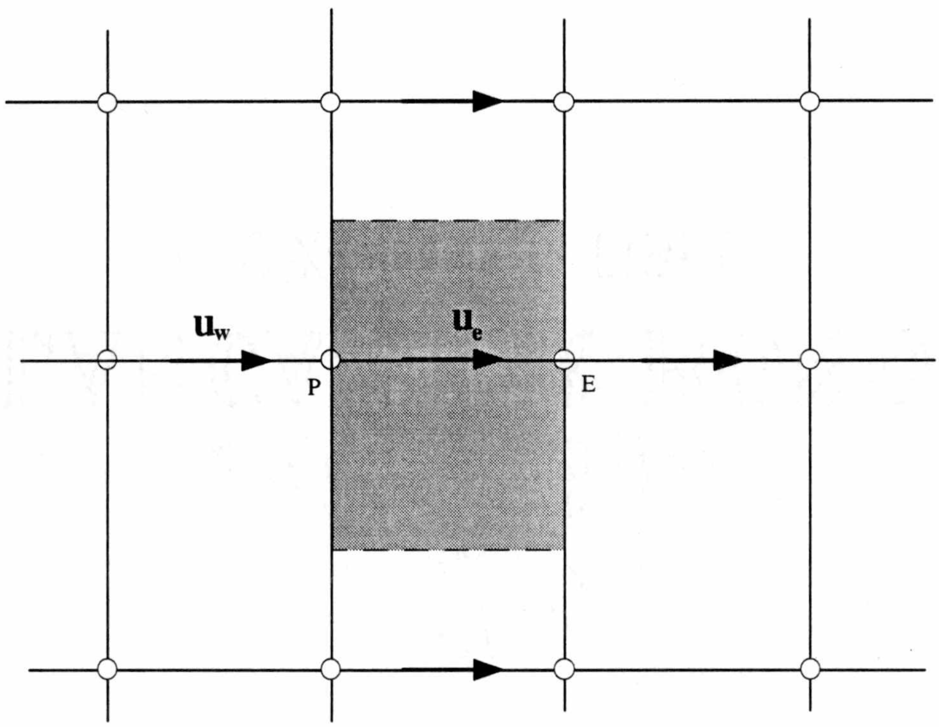

Figure 2.6 A staggered control volume for u

The * and ' velocity represent the guessed velocity and corresponding velocity corrections. By substituting these equations in the discretized momentum equations, the velocity-correction

equations become

$$u_e = u_e^* + d_e(p'_P - p'_E)$$
$$v_n = v_n^* + d_n(p'_P - p'_N) \quad (2.11)$$

where $d_e = \dfrac{\Delta y}{a_e}$, and $d_n = \dfrac{\Delta x}{a_n}$.

Substituting the velocity-correction equations in the discretized continuity equation, the following pressure correction equation is obtained:

$$a_P p'_P = a_E p'_E + a_W p'_W + a_N p'_N + a_S p'_S + b \quad (2.12)$$

where

$$a_E = \rho_e d_e \Delta y, \quad a_W = \rho_w d_w \Delta y$$
$$a_N = \rho_n d_n \Delta x, \quad a_S = \rho_s d_s \Delta x$$
$$a_P = a_E + a_W + a_N + a_S$$
$$b = \left[(\rho u^*)_w - (\rho u^*)_e\right]\Delta y + \left[(\rho v^*)_s - (\rho v^*)_n\right]\Delta x$$

The term b represents a "mass source." If b is zero, the starred velocities satisfy the continuity equation.

2.4.5. The Pressure Equation

To obtain the pressure field, the discretized momentum equations are written as

$$u_e = \hat{u}_e + d_e(p_P - p_E) \quad (2.13)$$

$$v_n = \hat{v}_n + d_n(p_P - p_N) \quad (2.14)$$

where

$$\hat{u}_e = \frac{\sum a_{nb} u_{nb} + b}{a_e} \text{ and } \hat{v}_n = \frac{\sum a_{nb} v_{nb} + b}{a_n}. \quad (2.15)$$

The pressure equation can be obtained by substituting equations (2.13) and (2.14) in the continuity equation. The final equations (2.13) and (2.14) are identical to the pressure correction equation (2.12) except $\hat{u}$, $\hat{v}$ replace u^*, v^*:

$$a_P p_P = a_E p_E + a_W p_W + a_N p_N + a_S p_S + b \tag{2.17}$$

2.5 Solution Method

The calculation procedure employed in this study is the SIMPLER algorithm[9] which consists of solving the pressure equation to obtain the pressure field and solving the pressure-correction equation to correct the velocity. The procedure can be summarized as:

1. Guess a velocity field. In this study a zero velocity field is used as the initial guess based on the physics of the flow where all velocities are zero prior to any flow development.
2. Calculate all coefficients of the discretized momentum equation; calculate $\hat{u}$ and $\hat{v}$ from Equation (2.15) by substituting the guessed velocity field as the neighbor velocities
3. Calculate the coefficient in the pressure equation and obtain the pressure field by solving the algebraic pressure equations represented by Equation (2.17).
4. Substitute the resulting pressure field in the discretized momentum equations to obtain an approximate velocity field by solving the momentum equations.
5. Substitute the resulting velocity field in the pressure correction Equation (2.12) and solve them to obtain the pressure correction.
6. Correct the velocity field by applying Equation (2.11) using corrected pressure.
7. Calculate the coefficients of discretized energy conservation equation by substituting the velocity field and solve it to obtain the temperature field.
8. Return to step 2 and repeat until all solutions converge.

9. Advance the time step and return to step 2 with final velocity field as guessed velocity field. Repeat until steady conditions are achieved.

2.6 Numerical Refinement Test

In order to select an appropriate grid size for the numerical computation, various grids from 5×4 to 20×40 are used. The mid point vertical velocity at the right symmetry axis in Case I with AR=2 and N_{CR}=2 is selected to compare the relative accuracy of various mesh sizes. Table 2.1 shows the actual value of the velocity for each mesh size and Table 2.2 shows the normalized velocity value relative to the velocity computed in the 20×40 grid taken as 1. For example, increasing the number of grid points from 10×10 to 20×40 results in an increase of 1.3 percent for the velocity. Figure 2.7 is a plot of results in Table 2.2. Assuming a 2 percent tolerance for accuracy (the dashed horizontal line), the figure shows that the mesh size larger than 10 in either x- or y-direction, provides solutions with acceptable accuracy.

For the computations in this study, nonuniform grids of 20×20 for Cases I and II, and 10×20 for Cases III and IV were selected. The mesh size near the wall was selected to be 60 percent smaller than corresponding uniform mesh size. The choice of a nonuniform mesh size adds to the numerical accuracy due to large velocity gradients near the walls

2.7 Code Validation

The computer code developed for this study is used to solve a problem with known velocity field. This made it possible to verify the code and add confidence to the numerical procedure used in solving the problems in Cases I through IV. The problem considered for the application of the code is illustrated in Figure 2.8. An infinite vertical plate with an arbitrary surface temperature is in contact with an isothermal quiescent fluid. Assuming

Table 2.1 Variation of the selected velocity for an M×N grid

M	N			
	4	10	20	40
5	0.550258	0.557774	0.558698	0.559
10	0.576662	0.583572	0.584342	0.58462
20	0.583336	0.590088	0.590778	0.590994

Table 2.2 Comparison of the relative velocities

M	N			
	4	10	20	40
5	0.931072	0.94379	0.945353	0.945864
10	0.975749	0.987441	0.988744	0.989215
20	0.987042	0.998467	0.999635	1

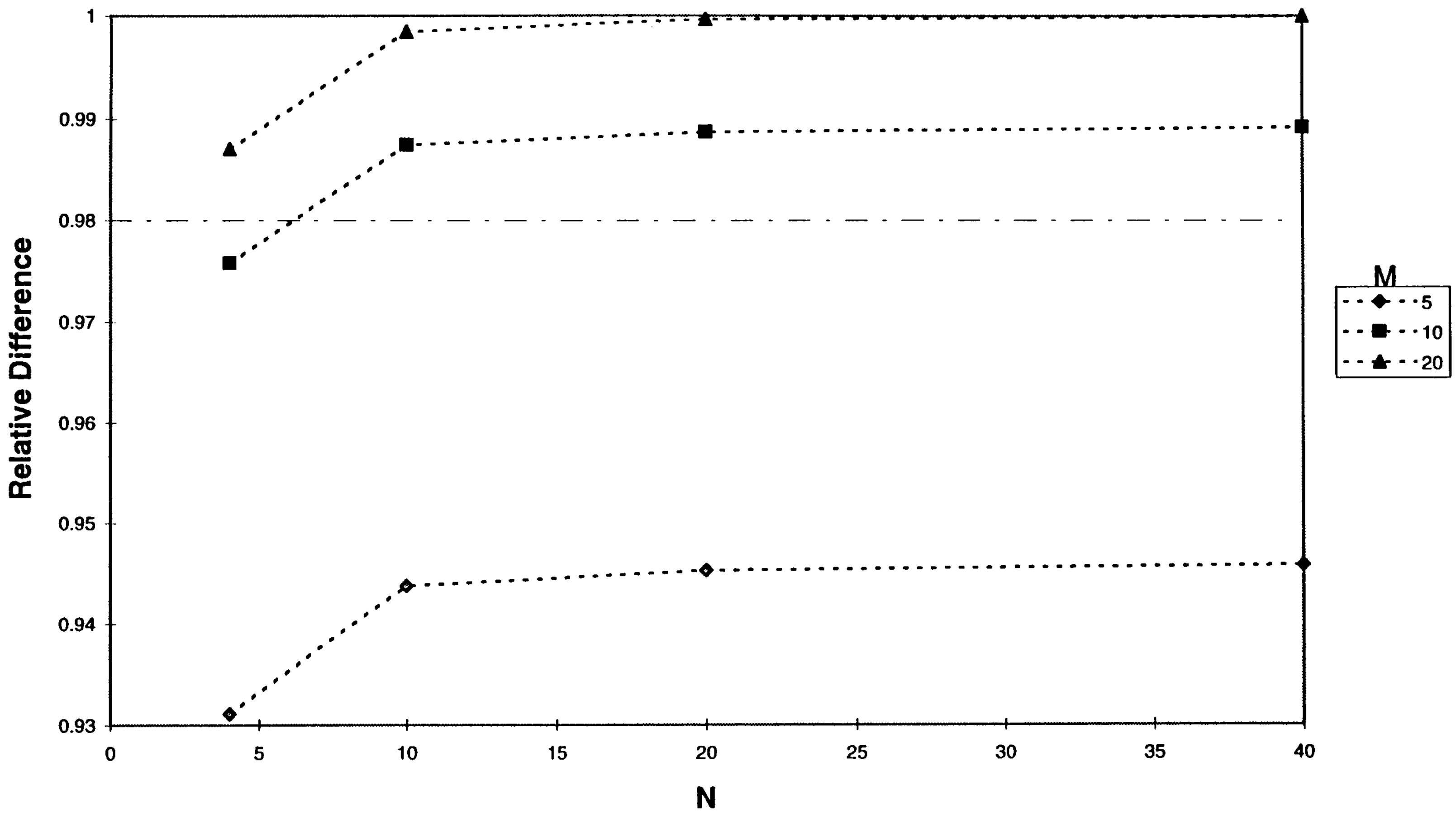

Figure 2.7 Relative difference of velocity values as compared to grid 20×40

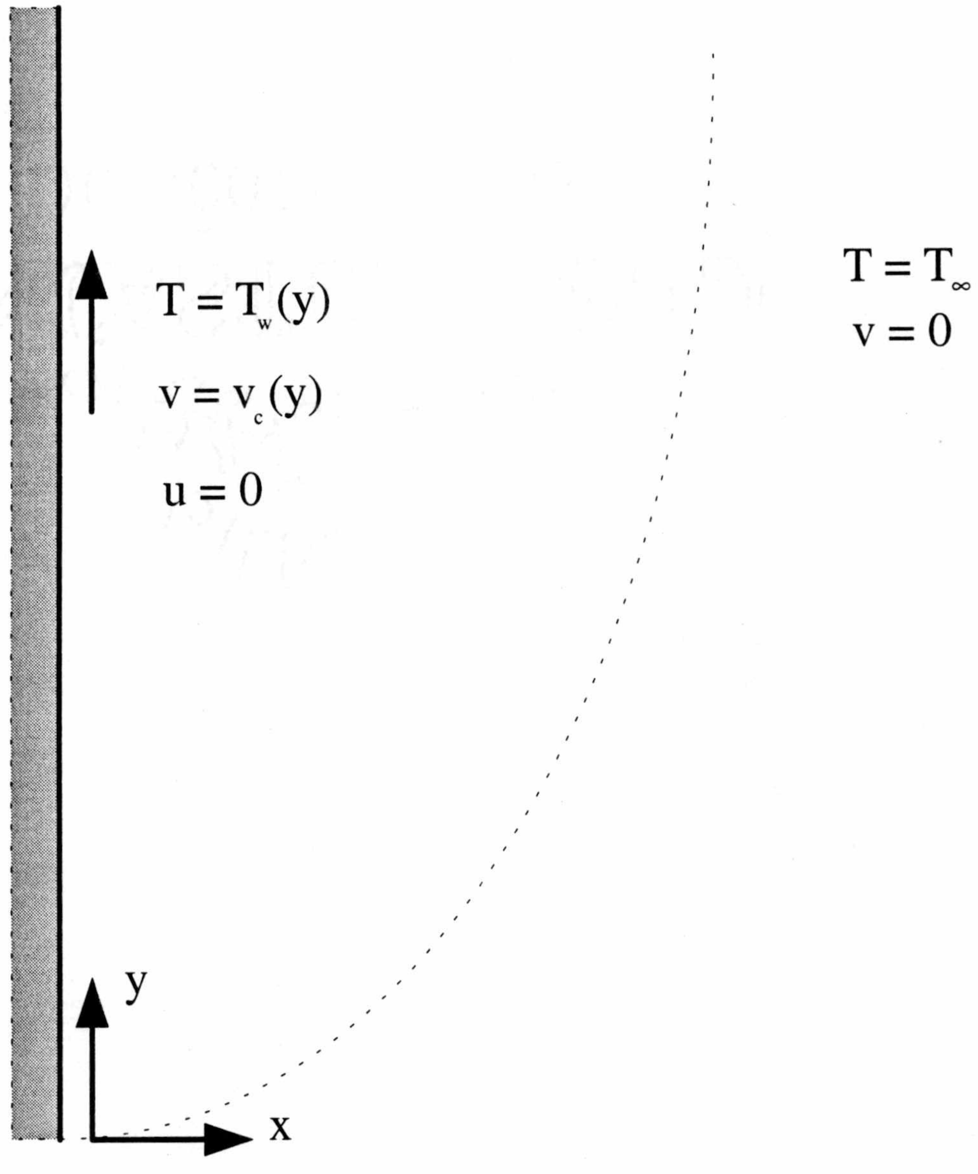

Figure 2.8 The boundary conditions of the infinite vertical wall

steady, laminar, and a constant-property fluid and using Boussinesq and boundary-layer approximations, the resulting governing equations are[7]:

$$\frac{\partial u}{\partial x}+\frac{\partial v}{\partial y}=0$$

$$u\frac{\partial v}{\partial x}+v\frac{\partial v}{\partial y}=\nu\frac{\partial^2 v}{\partial x^2}+g\beta(T-T_\infty)$$

$$u\frac{\partial T}{\partial x}+v\frac{\partial T}{\partial y}=\alpha\frac{\partial^2 T}{\partial x^2}$$

The boundary conditions are

$$u=0,\ v=v_c(y),\ T=T_w(y)\ \text{at}\ x=0$$

$$v\to 0,\ T\to T_\infty\ \text{when}\ x\to\infty$$

where $v_c(y)$ is the thermal creep flow velocity on the wall given by Equation (1.1) and $T_w(y)$ is a specified wall temperature distribution.

For the special wall temperature profile $T_w = T_\infty + Ny^3$, the following similarity variable

$$\eta=\frac{x}{y}\sqrt{\frac{Re_y}{2}}$$

where

$$Re_y=\frac{v_c y}{\nu}=\frac{3c_s N y^3}{T_\infty}$$

and the dependent variables defined as

$$v=\frac{\nu}{y}Re_y f'$$

$$u=-\frac{\nu}{y}\sqrt{\frac{Re_y}{2}}[3f+\eta f']$$

$$(T - T_\infty) = (T_w - T_\infty)\theta(\eta)$$

result in transforming the governing equations to

$$f''' + 3ff'' - 4(f')^2 + (Gr/Re^2)\theta = 0$$
$$\theta'' + Pr[3f\theta' - 6f'\theta] = 0$$

where

$$Gr = \frac{g\beta N x^6}{\nu^2} \text{ and } \frac{Gr}{Re^2} = \frac{gT_\infty}{9c_s^2 N \nu^2}.$$

with dimensionless boundary conditions given by

$$\text{when } \eta = 0,\ f = 0, f' = 1,\ \theta = 1$$
$$\text{as } \eta \to \infty,\ f' \to 0,\ \theta \to 0$$

Figure 2.9 is a plot of the dimensionless velocity f' vs. η for Gr/Re^2 ranging from 1 to 100 when $Pr = 0.7$ from reference [7]. This "exact" solution can be used to verify the developed code. For this purpose, this problem was solved using the code developed for the solution of discretized Equations (2.8). The unsteady governing equations were solved for long real times until steady solutions were obtained. The similarity variable was calculated from the resulting velocity and temperature and used in the graphical presentation of the results for comparison purposes.

The infinite spatial aspect of the problem is modeled in the code by imposing boundary conditions far away from the flow domain under consideration. The farther from the interested domain the location on which the boundary conditions are imposed, the better the results represent the known solution (Figure 2.9) for this infinite vertical wall case.

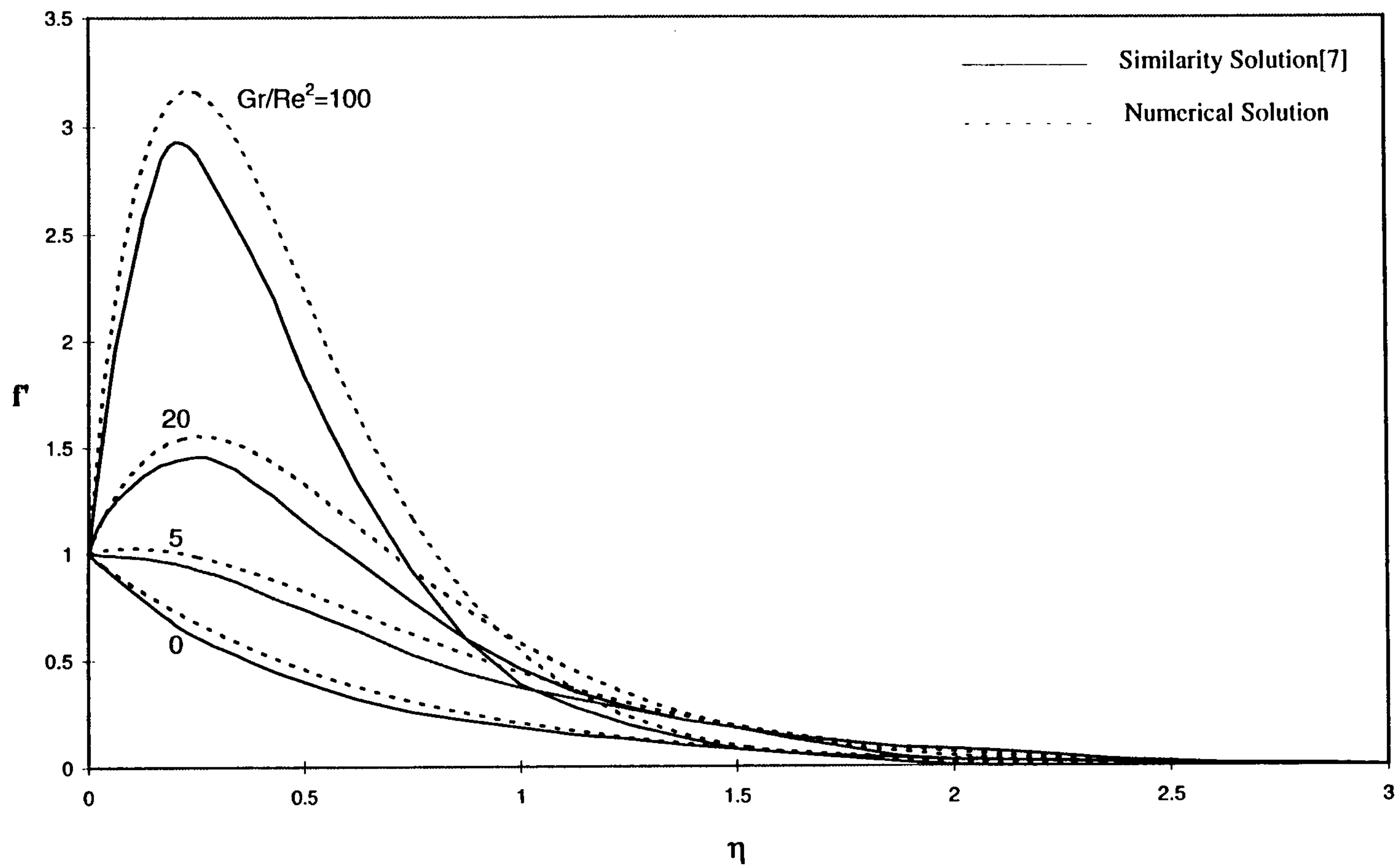

Figure 2.9 The dimensionless vertical velocity, f' as a function of distance normal to the wall, η .

Numerical solutions of normalized vertical velocity f' are presented and compared with similarity solutions in Figure 2.9 for Gr/Re^2 ranging from 1 to 100. A finite computation domain was selected containing the heated plate with a height 3H and a width L=9H as shown in Figure 2.10. A uniform grid of 30×30 was used over this domain. At the boundary DC (see Figure 2.10), the flow was taken as the infinity condition. Also, the normal gradients of velocity and temperature along the boundary AD, were set at zero. This means that the velocity and the temperature above AD were assumed to be the same as the values along the boundary AD. The infinite physical domain was modeled by a finite computation domain by limiting the wall creep with creep flow to two isothermal walls on each side (AE and BF). In these extended wall regions, no creep flow is expected and no-slip velocity boundary condition can be assumed. The resulting no-slip velocity and uniform temperature boundary conditions on boundaries AE and BF are shown in Figure 2.10. Despite these necessary approximate assumptions, the results are found quite close to the similarity solutions. The numerical solutions are slightly higher than similarity solutions with a maximum of 9.6% deviation between two results which occurs at the largest Gr/Re^2 value. The main reason for the deviations is that a finite computation domain must be selected to replace an infinite domain. In addition, a relatively coarse grid size was selected near the vertical left wall where the flow is being driven. Since the velocity field increases with increasing Gr/Re^2, the error also increases with Gr/Re^2 as expected. For Gr/Re^2 larger than 100, a finer grid size near the wall and a larger width of computation domain should be used. However, these larger values are not applicable to microgravity conditions and there was no need to carry out the computation beyond this range of Gr/Re^2 values.

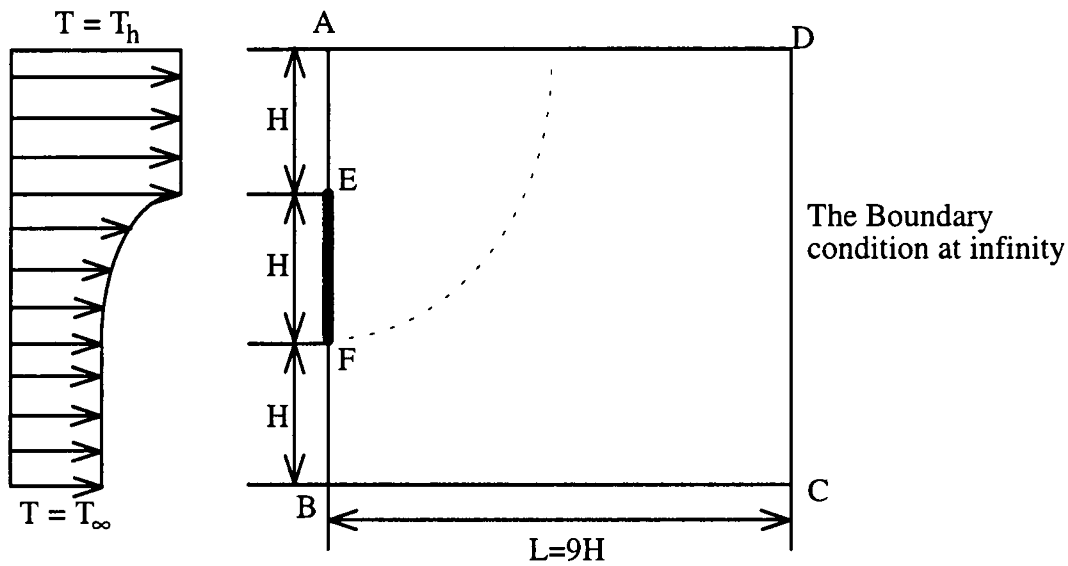

Figure 2.10 The computation domain of the infinite vertical wall

Chapter 3
RESULTS AND DISCUSSION

3.1 Linear Sidewall Temperature with Other Walls Insulated (Case I)

The results for Case I are presented for AR=1 and N_{CR}=1.5 and for three values of Grashof numbers: zero (pure thermal creep flow), 750 and 3000. As stated earlier, in all the results which will follow the Prandtl number was selected to be 0.72

3.1.1 Flow Patterns

The flow patterns are shown for two Grashof numbers in Figures 3.1 and 3.2. At a Grashof number of zero, there is only a single counterclockwise-rotating eddy because thermal creep alone is driving the flow and the direction of the motion is the negative y-direction. Figure 3.1 shows the flow velocity vector at a Grashof number of 750. At the right bottom corner, where the flow field is farthest from the influence of thermal creep, the flow field is beginning to be affected by the buoyancy force.

At a Grashof number of 3000, the effect of buoyancy is strong enough to alter the flow pattern significantly, and there is rough parity between buoyancy and thermal creep effects. Two cells appear distinctly as shown in Figure 3.2. The fluid above the middle horizontal line is observed to move counterclockwise and is dominated by thermal creep. The lower portion moves clockwise and the effect of thermal creep near the left wall is effectively countered by the buoyancy force.

3.1.2 Centerline Velocity Profile Along the Center Vertical Plane

Figure 3.3 shows the normalized horizontal component of velocity along the center vertical plane, X=0.5, for Grashof numbers of 750 and 3000. For Gr=750, the results

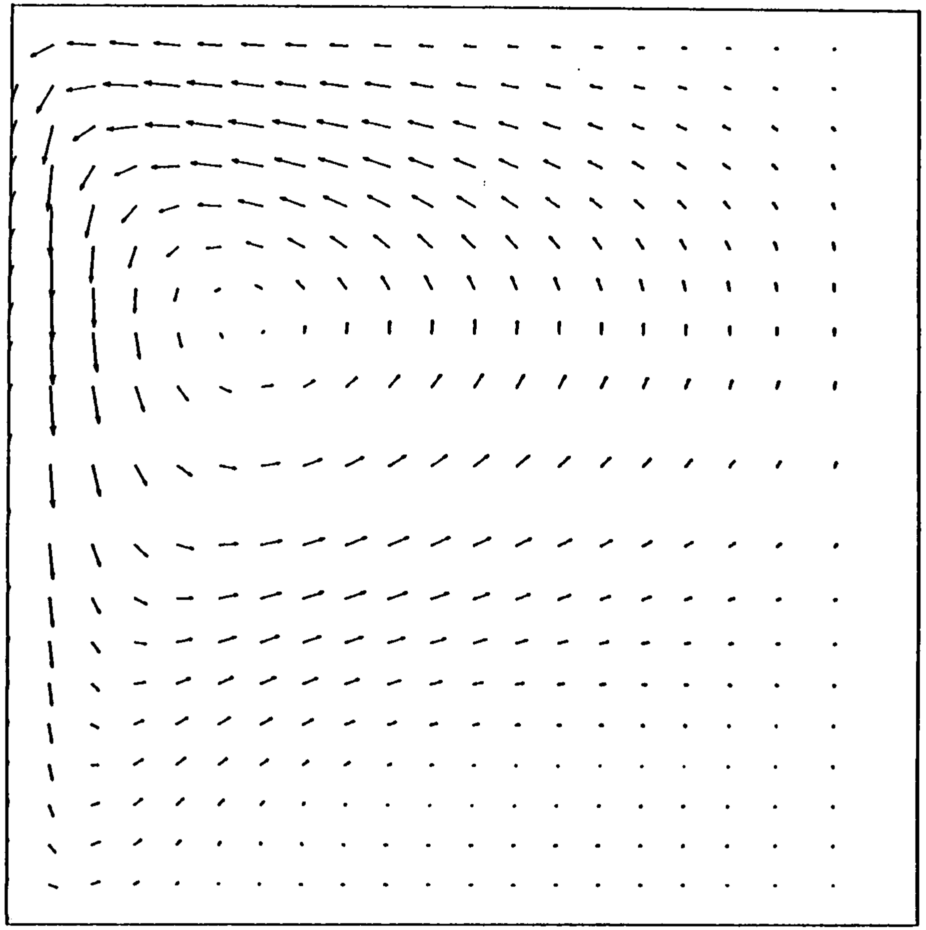

Figure 3.1 Velocity vector plot for Case I (AR=1.0, Ncr=1.5, Gr=750)

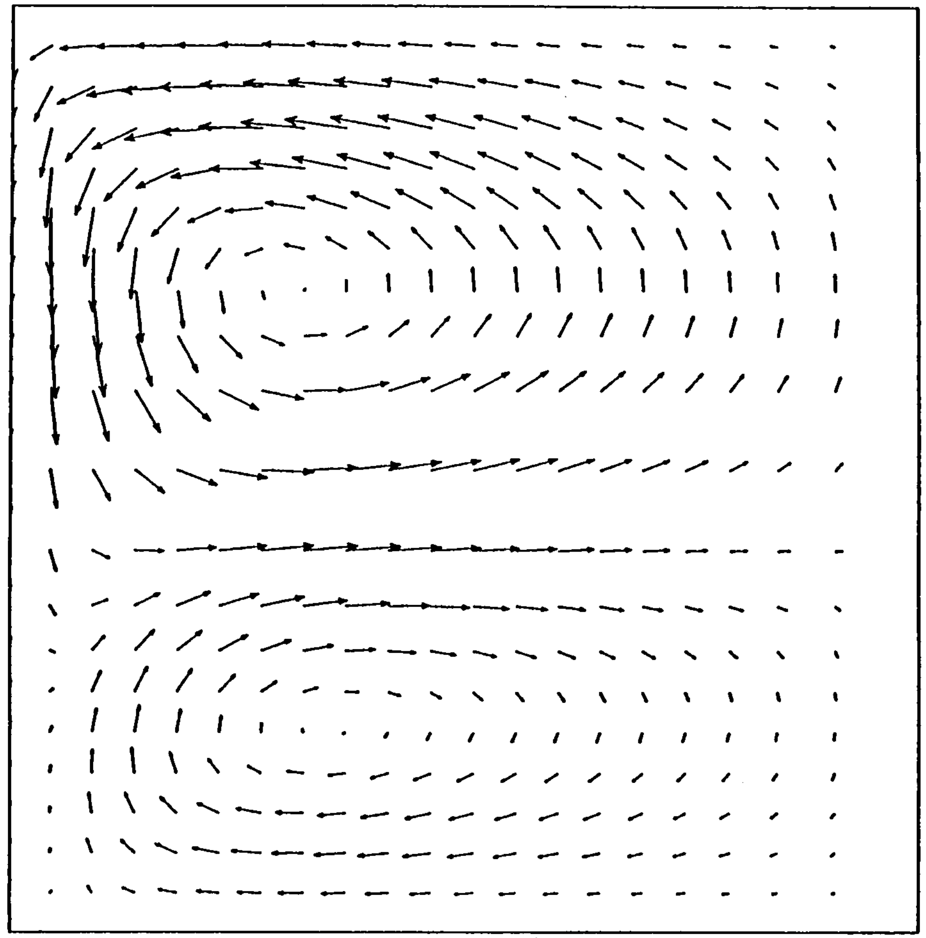

Figure 3.2 Velocity vector plot for Case I (AR=1.0, Ncr=1.5,Gr=3000)

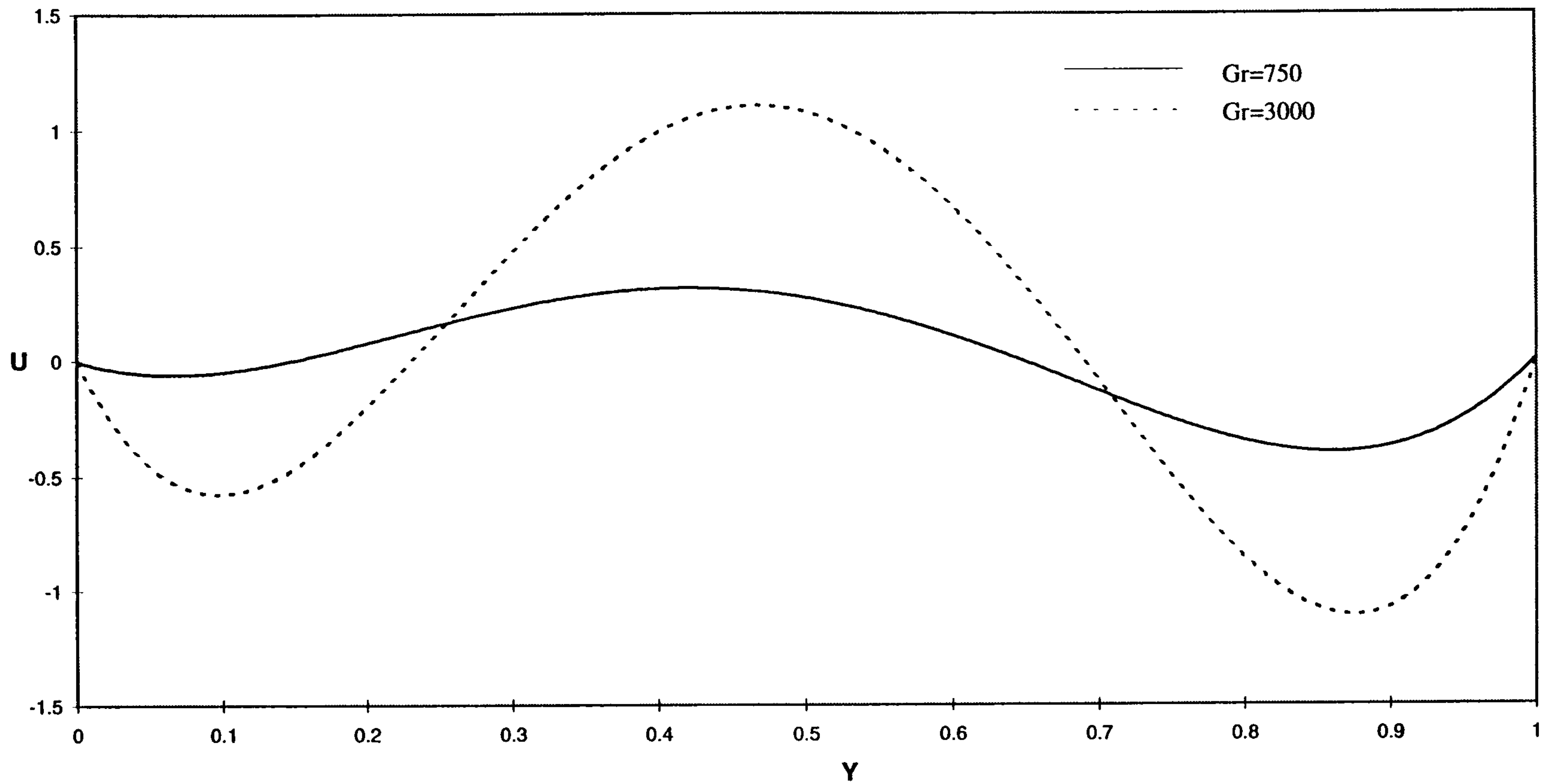

Figure 3.3 The horizontal velocity profile along the middle vertical plane of the enclosure (Case I)

indicate the presence of weak flow in the region of $Y \leq 0.15$, which is mainly due to buoyancy. This influence grows as Grashof number becomes larger. The result for Gr=3000 shows that the buoyancy-dominated region is expanded from $Y \leq 0.15$ to $Y \leq 0.45$ and the highest velocity is at the contact region between two cells where the buoyancy and thermal creep effects combine and reinforce each other. As the Grashof number increases, the buoyancy dominated region will be extended upward, and eventually a single eddy structure will replace the two-cell flow when the Grashof number reaches large values.

3.1.3 Isotherms

Despite the complexity of the flow pattern, the heat transfer to the flow remains dominated by the conduction mode and convective effects are observed to be secondary. For example, for Gr=3000, the normalized velocity, which is local Reynolds number, is less than 1.3. Figures 3.4 and 3.5 show the isotherms at Gr=750 and 3000, respectively. The results are very close to the results of the pure conduction problem in which the isotherms are symmetric with respect to the middle horizontal line, Y=AR/2. The only difference is that in this case the isotherms are shifted slightly upward.

Since the left sidewall is the only non-isothermal wall, energy is supplied and removed only at this wall. Isotherms in Figures 3.4 and 3.5 suggest that energy is supplied to the flow through the lower half of the left wall and is removed through the upper half. Since net energy flow is zero, the average Nusselt number at this wall is also zero.

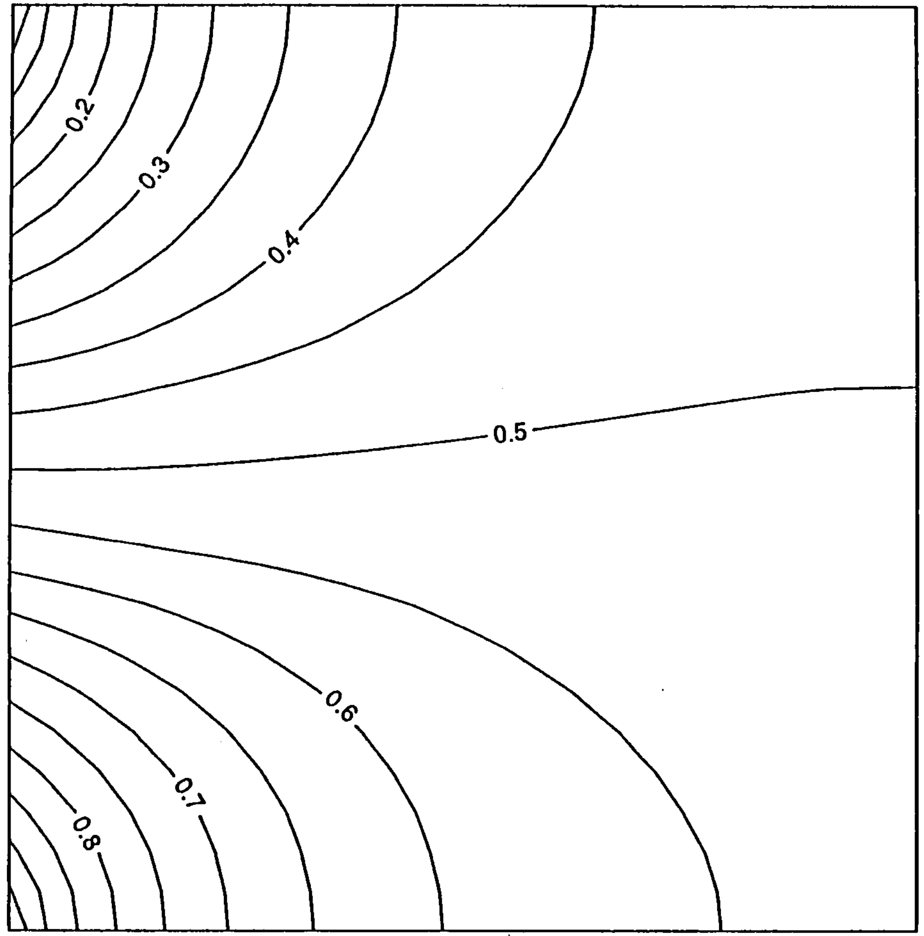

Figure 3.4 Isotherms for Case I (AR=1.0, Ncr=1.5, Gr=750)

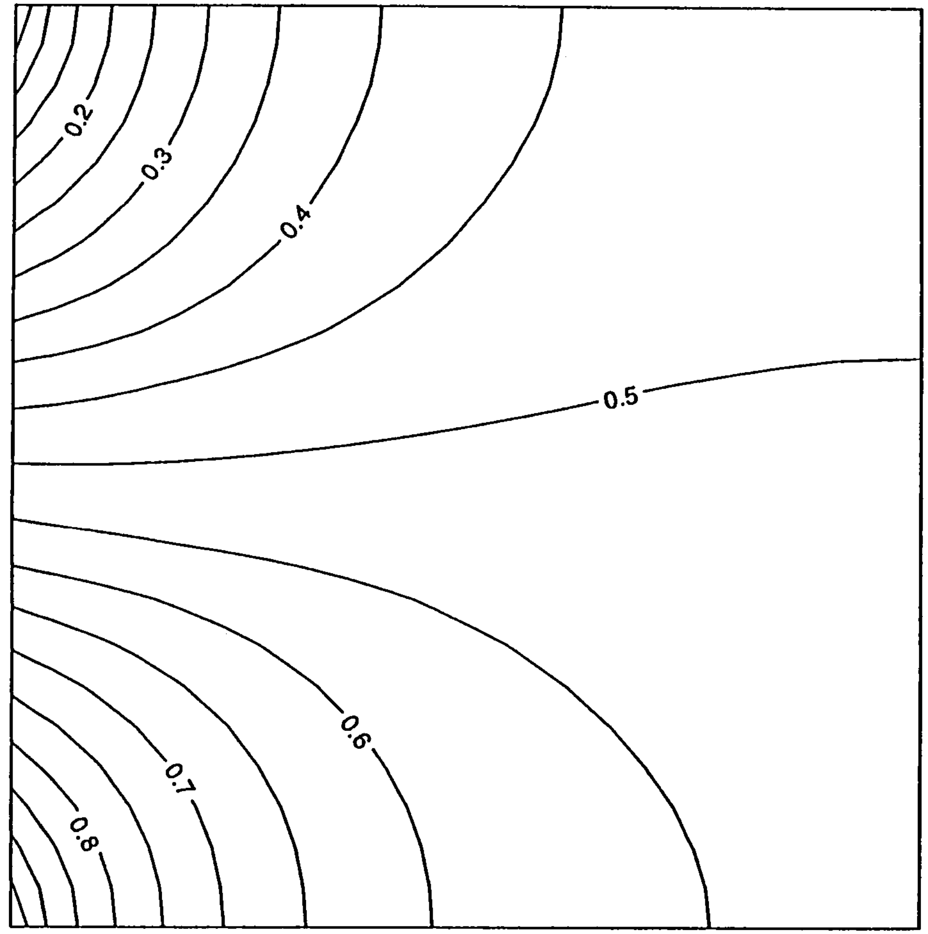

Figure 3.5 Isotherms for Case I (AR=1.0, Ncr=1.5, Gr=3000)

3.2 A Nonlinear Sidewall Temperature with Other Walls Insulated (Case II)

The results for Case II are presented for AR=1.0 and N_{CR}=2.0 and two values of Grashof numbers: zero and 2000.

3.2.1 Flow Pattern

The boundary condition in Case II was selected as an example of thermal creep on two walls where they would reinforce each other. At the left sidewall, thermal creep drives fluid in the negative direction, feeding the positive flow direction on the right side. When other influences are eliminated, thermal creep drives the entire flow counterclockwise in a single cell structure as shown in Figure 3.6. The fluid motion is strongest near the bottom left and upper right regions of the enclosure.

In the presence of gravity, the fluid is influenced by buoyancy forces in addition to the creep flow. Because the direction of gravity is downward, the fluid at the lower left corner is expected to move upward and the fluid at the upper right corner is expected to move leftward. Thus, two effects create two cells as shown in Figure 3.7. In the upper cell, the buoyancy and thermal creep phenomenon reinforce and aid each other and, as a result, a strong counterclockwise circulation is observed. In the lower cell, two effects oppose each other. Near the left wall the downward flow driven by thermal creep is stronger than the upward flow driven by buoyancy and far from the left wall, the opposite is true. As a result, the upper cell is extended to the left lower corner and the lower cell is reduced in size and restricted to the lower right corner of the enclosure as shown in Figure 3.7.

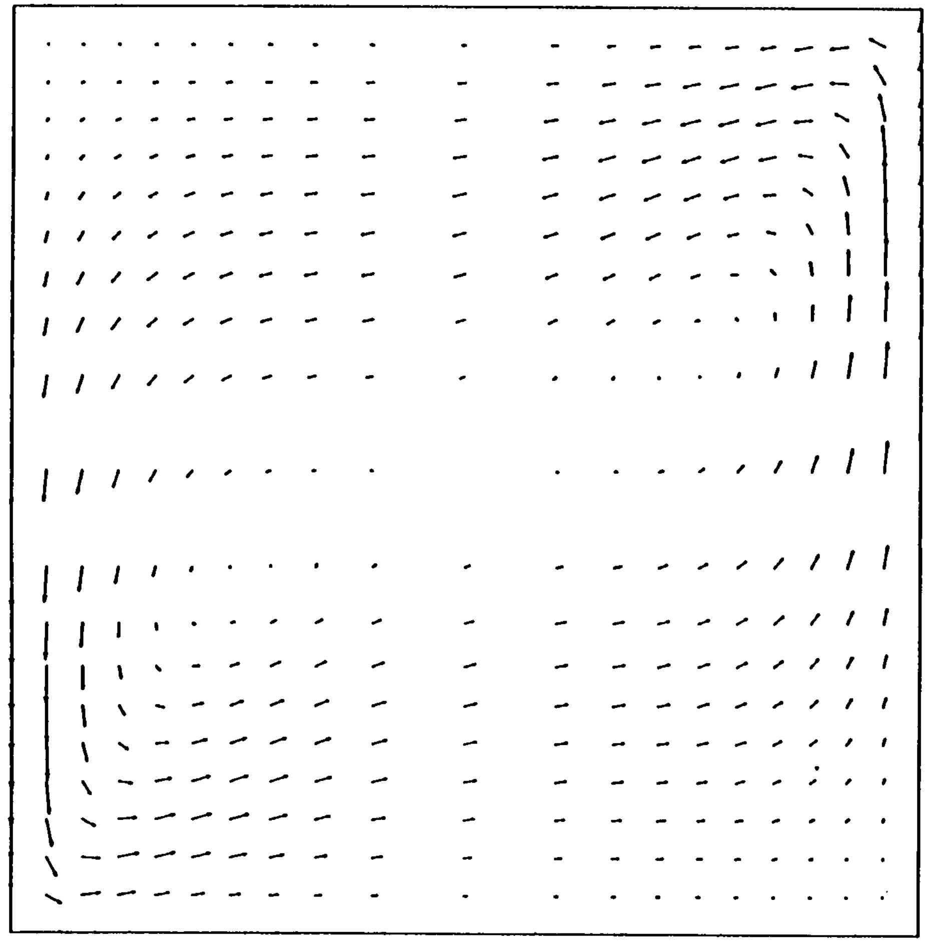

Figure 3.6 Velocity vector plot for Case II (AR=1.0, Ncr=2.0, Gr=0)

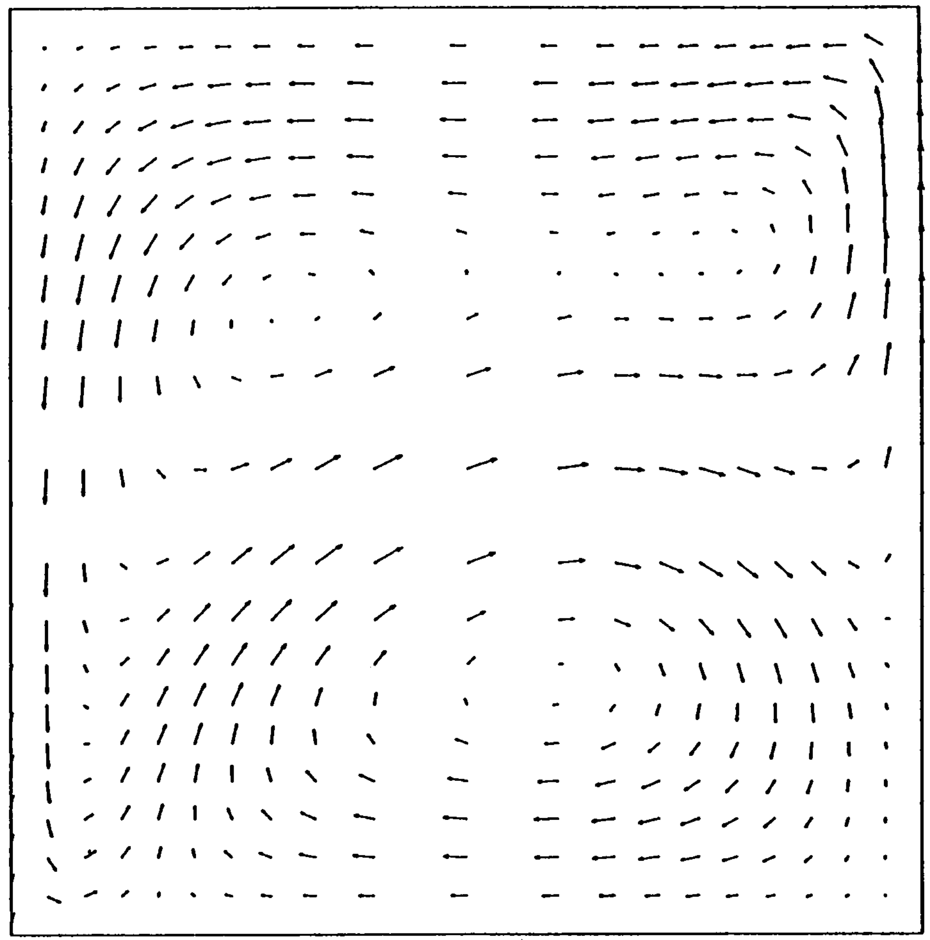

Figure 3.7 Velocity vector plot for Case II (AR=1.0, Ncr=2.0,Gr=2000)

3.2.2 Velocity Profile Along the Center Vertical Plane

The normalized horizontal velocity is calculated along the center vertical plane, X=0.5, for Grashof numbers of 0 and 2000 and is presented in Figure 3.8 (a). The magnitude and the direction of the velocity are very similar to Case I. However, it should be noted that the flow patterns are different. For Gr=0, the velocity is symmetrical in respect to the center point because of the nature of the boundary conditions and the absence of buoyancy effects. For Gr=2000, a prominent rightward horizontal velocity is observed which is almost three times the flow in the absence of gravity. The nature of the velocity profile and its symmetry are also observed to have changed.

Figure 3.8 (b) shows the normalized vertical velocity along the horizontal plane Y=0.25AR. For Gr=0, the entire flow is driven by opposing creep flow velocities on the two vertical walls. Near the left wall the down flow is strong and a boundary-layer type region is observed due to the strong creep velocity. The rest of the enclosure is filled by a weak upward flow which is accelerating upward near the right wall. For Gr=2000, the creep velocity at the left wall is strong enough to preserve the counterclockwise motion in the region near the left wall ($X \leq 0.23$) and the buoyancy principally drives the flow in the rest of region except very near the right wall ($X \geq 0.97$) where the velocity vector changes the sign again due to a weaker upward creep velocity. It is noted that the effect of thermal creep remains limited to the region near the wall for large Grashof number as illustrated by velocity profile near the right wall in Figure 3.8 (b).

3.2.3 Isotherms

Similar to Case I, the flow in this case is not strong enough to significantly affect heat transfer, and the heat transfer is dominated by conduction. In a pure conduction case, the isotherms should be symmetric relative to the center point. However, because of the

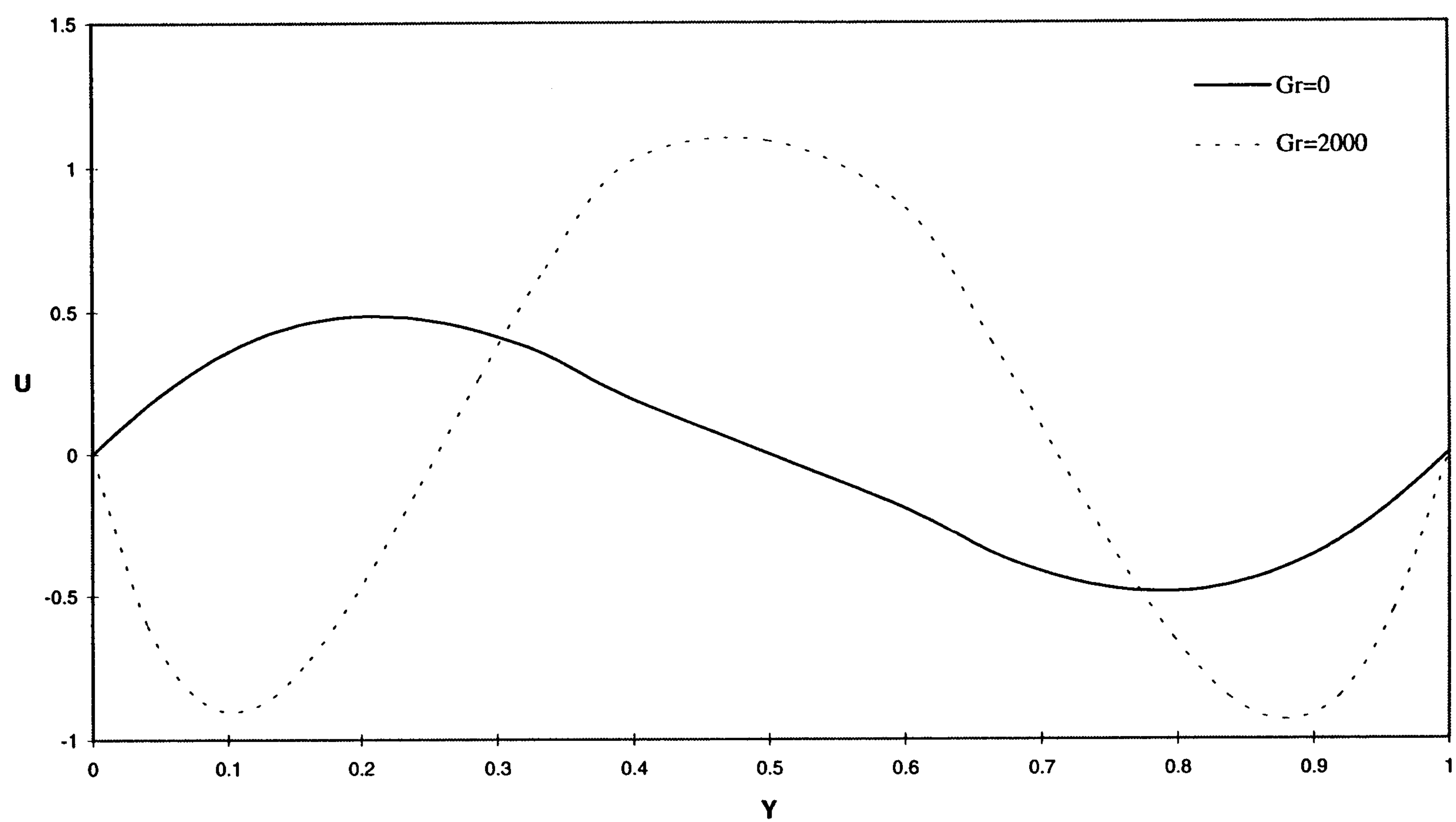

(a) The horizontal velocity profile at midsection, X=0.5

Figure 3.8 The velocity profile (Case II)

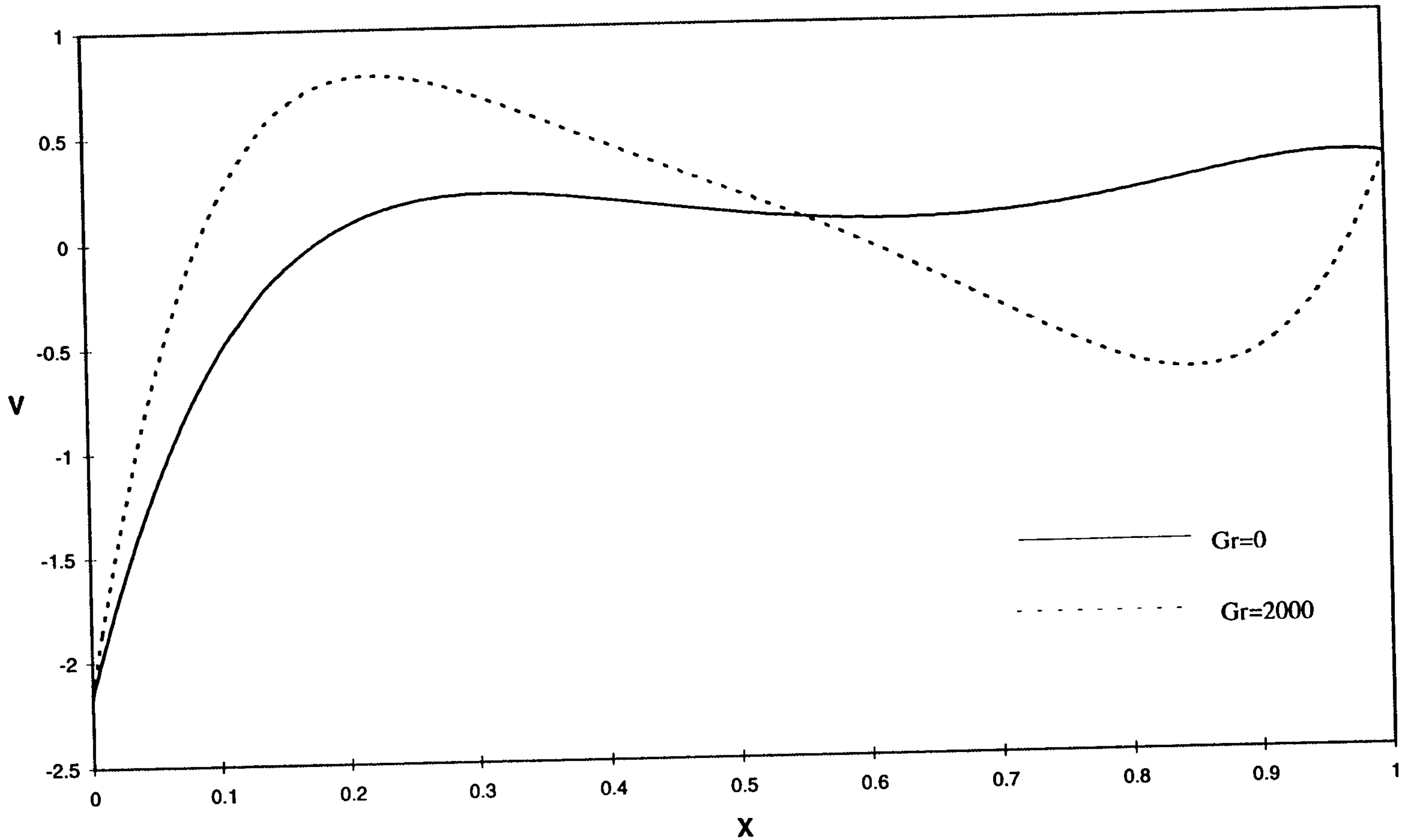

(b) The vertical velocity profile at cross section, Y=0.25AR

Figure 3.8 (continued)

flow driven by thermal creep, the isotherms are observed to have rotated slightly in the counterclockwise direction. This is illustrated in Figures 3.9 and 3.10. In all cases, heat transfer within the range of Grashof number considered in this study remains similarly dominated by conduction and similar corresponding isotherm patterns are observed.

Since imposed temperature distribution on the left wall is symmetric to that on the right wall in respect to the middle point of the enclosure and the other walls are insulated, the overall heat flux is zero like Case I. Therefore, the average Nusselt numbers at the left and right walls become zero.

3.3 Linear Sidewall Temperature Distribution with Isothermal Horizontal Walls (Case III)

The results for Case III are presented for AR=2.0 and N_{CR}=1.5 and selected various values Grashof number from zero to 2000.

3.3.1 Flow Pattern

In this case thermal creep drives the fluid downward near the left wall. As expected, for Gr=0 one counterclockwise circulation fills the entire cavity as shown in Figure 3.11. Since the wall temperature is higher at the lower-end of the enclosure, the buoyancy force drives the fluid upward near the left wall opposing imposed creep flow. Depending on the relative strength of these two effects, the entire flow can be dominated by one or the other. In small or zero gravity, the circulation is counterclockwise because the flow is dominated by thermal creep. The buoyancy begins to dominate the flow after a critical Grashof number (approximately 1600) is achieved. Figures 3.12 and 3.13 show the velocity field just before and after critical Grashof number, respectively. It is observed that for Grashof number below the critical value the flow circulation remains counterclockwise

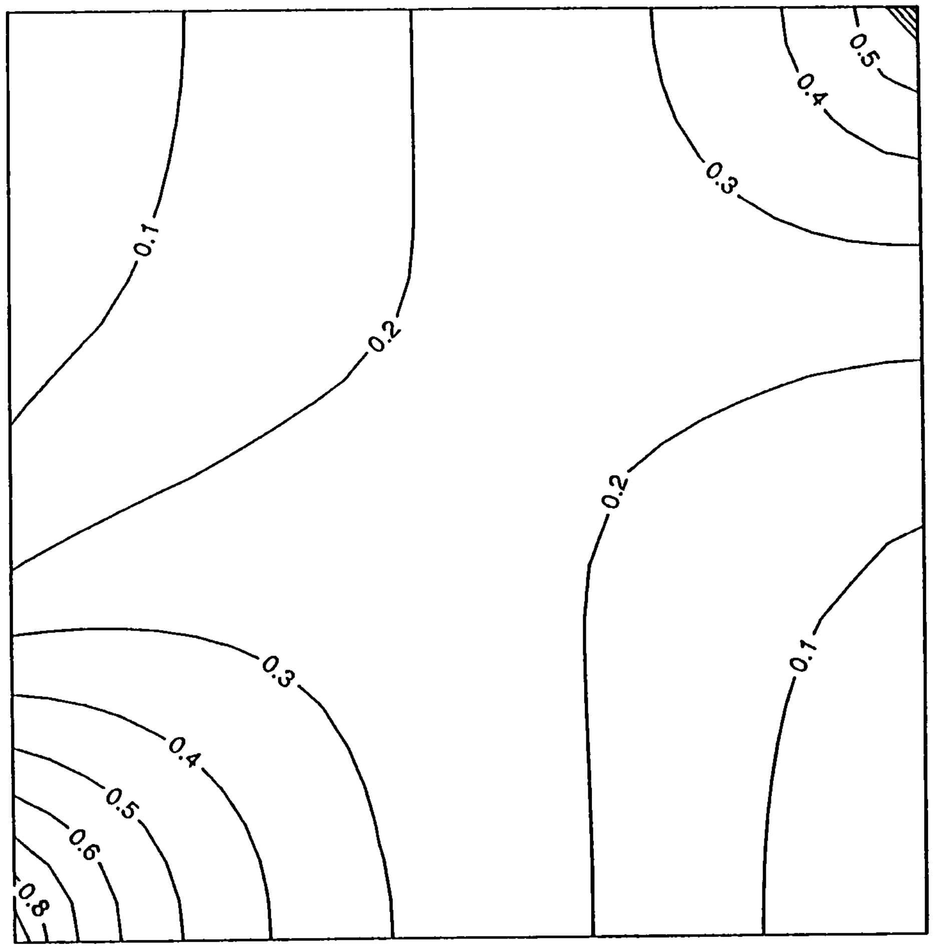

Figure 3.9 Isotherms for Case II (AR=1.0, Ncr=2.0, Gr=0)

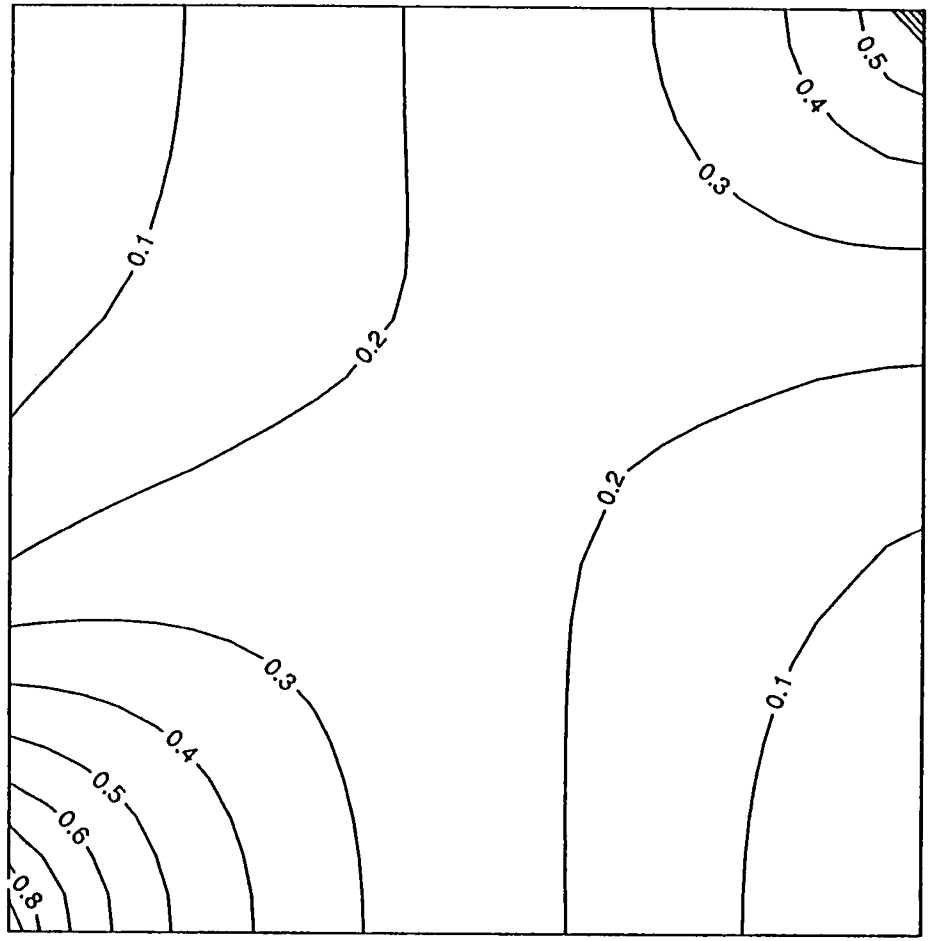

Figure 3.10 Isotherms for Case II (AR=1.0, Ncr=2.0, Gr=2000)

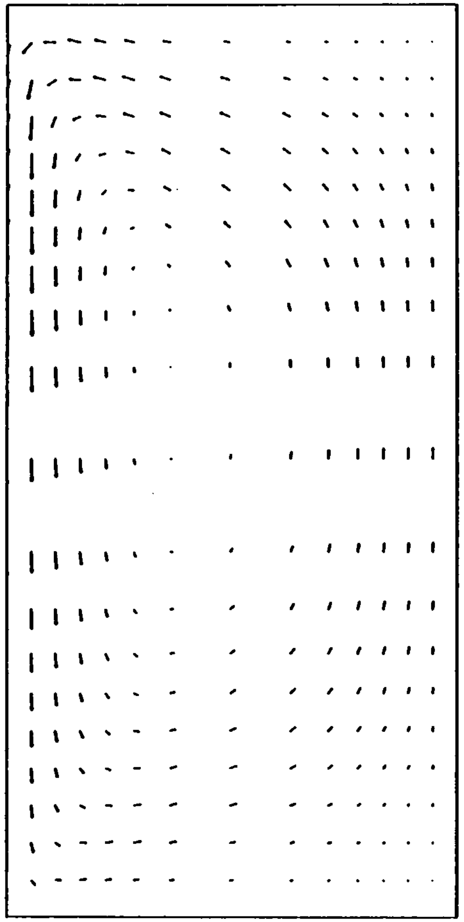

(a) Velocity vector plot

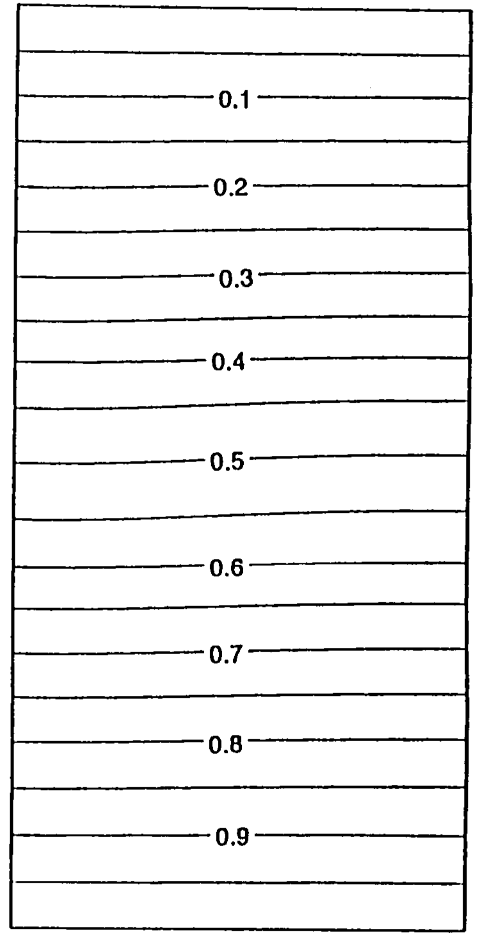

(b) Isotherms

Figure 3.11 Velocity vector plot and isotherms for Case III (AR=2.0, Ncr=1.5, Gr=0)

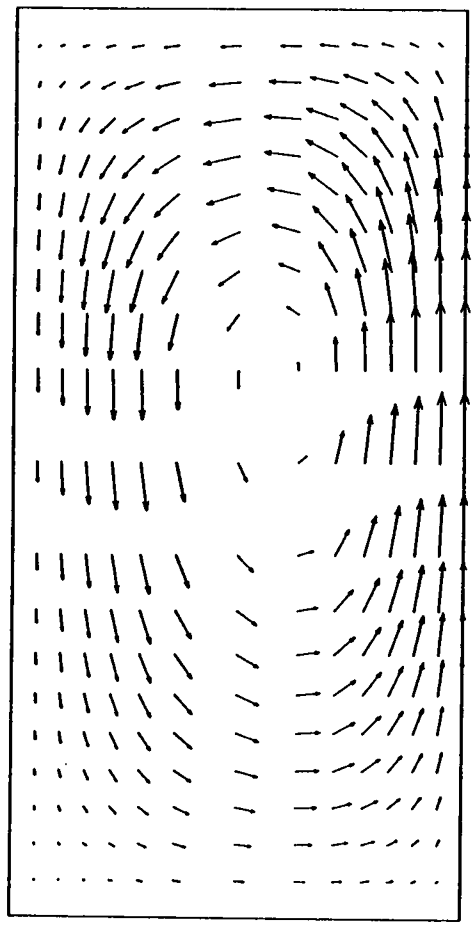

(a) Velocity vector plot

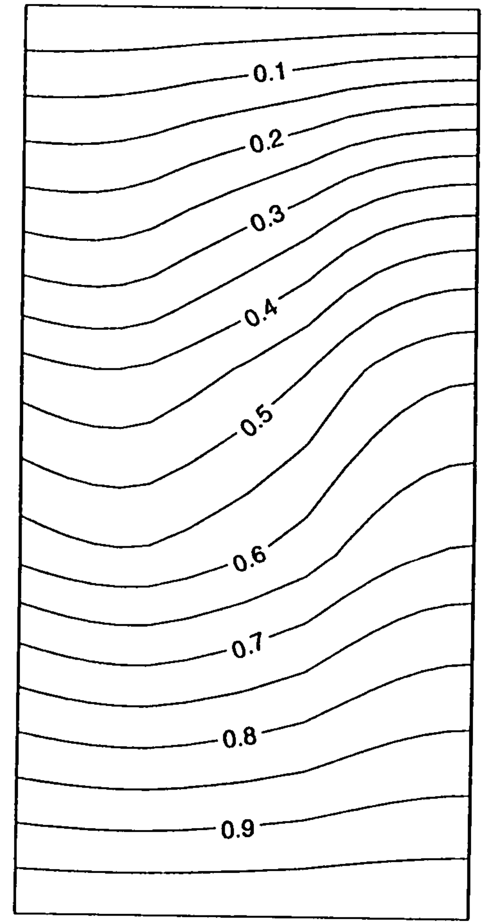

(b) Isotherms

Figure 3.12 Velocity vector plot and isotherms for Case III (AR=2.0, Ncr=1.5, Gr=1598)

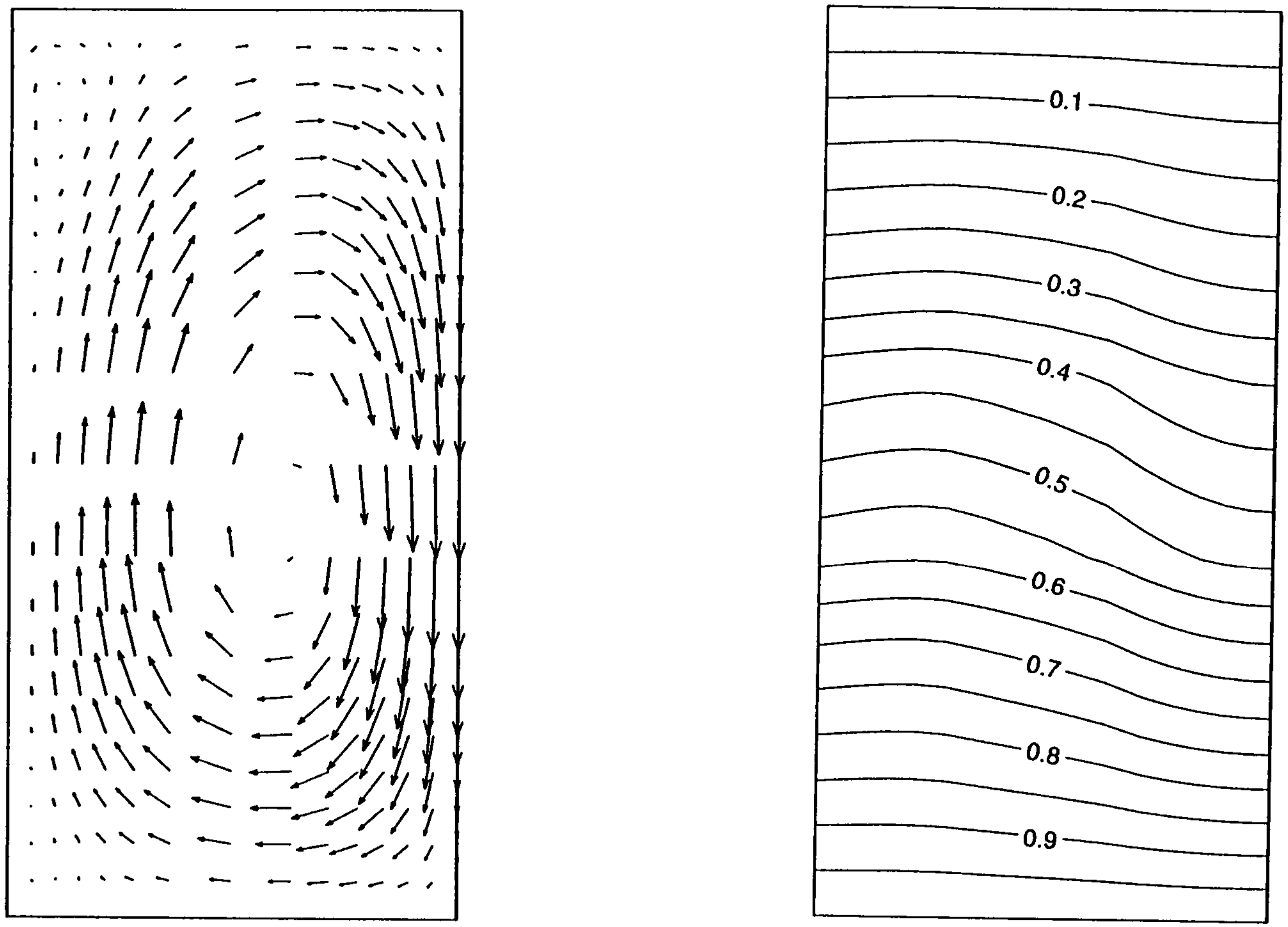

(a) Velocity vector plot

(b) Isotherms

Figure 3.13 Velocity vector plot and isotherms for Case III (AR=2.0, Ncr=1.5, Gr=1601)

as established by the creep flow. As the Grashof number increases and approaches the critical value, the buoyancy effect seems to "assist" thermal creep and large flow velocities are generated as shown in Figure 3.12. It is noticed that the magnitude of the velocity field continues to increase as Grashof number increases. Immediately after the critical Grashof number the flow structure is suddenly changed. The flow direction is predominately clockwise with a small remnant of a weak counterclockwise cell still observable in Figure 3.13. However, the weak cell rapidly disappears as Grashof number increases and the effect of thermal creep remains limited very near the left wall as illustrated in Figure 3.14.

Between Gr=1300 and 1610 a transient unstable regime is observed in which also the direction of circulation suddenly changes. In this range of Grashof number, the two competing buoyancy and creep effects oppose each other with comparable strengths and the flow is unstable and numerical convergence is achieved with difficulty. For example, the CPU requirement for Gr=1598 is larger than a factor of ten as compared with Gr=0.

3.3.2 Vertical Velocity Profile at Center Horizontal Plane

The vertical component of velocity at center horizontal plane, Y=0.5AR, is depicted in Figure 3.15. As mentioned, the magnitude of velocity keeps growing as Grashof number changes from 0 to 1607 until a sudden direction change of velocity which occurs at around $Gr_c=1600$. This sudden change at the critical Grashof number is illustrated clearly in the figure.

3.3.3 Isotherms and Heat Transfer

Similar to the other cases, heat transfer to the flow remains dominated by the conduction mode at small Grashof number. As shown in Figure 3.11, temperature is changing linearly from the lower to the upper wall very similar to a pure conduction

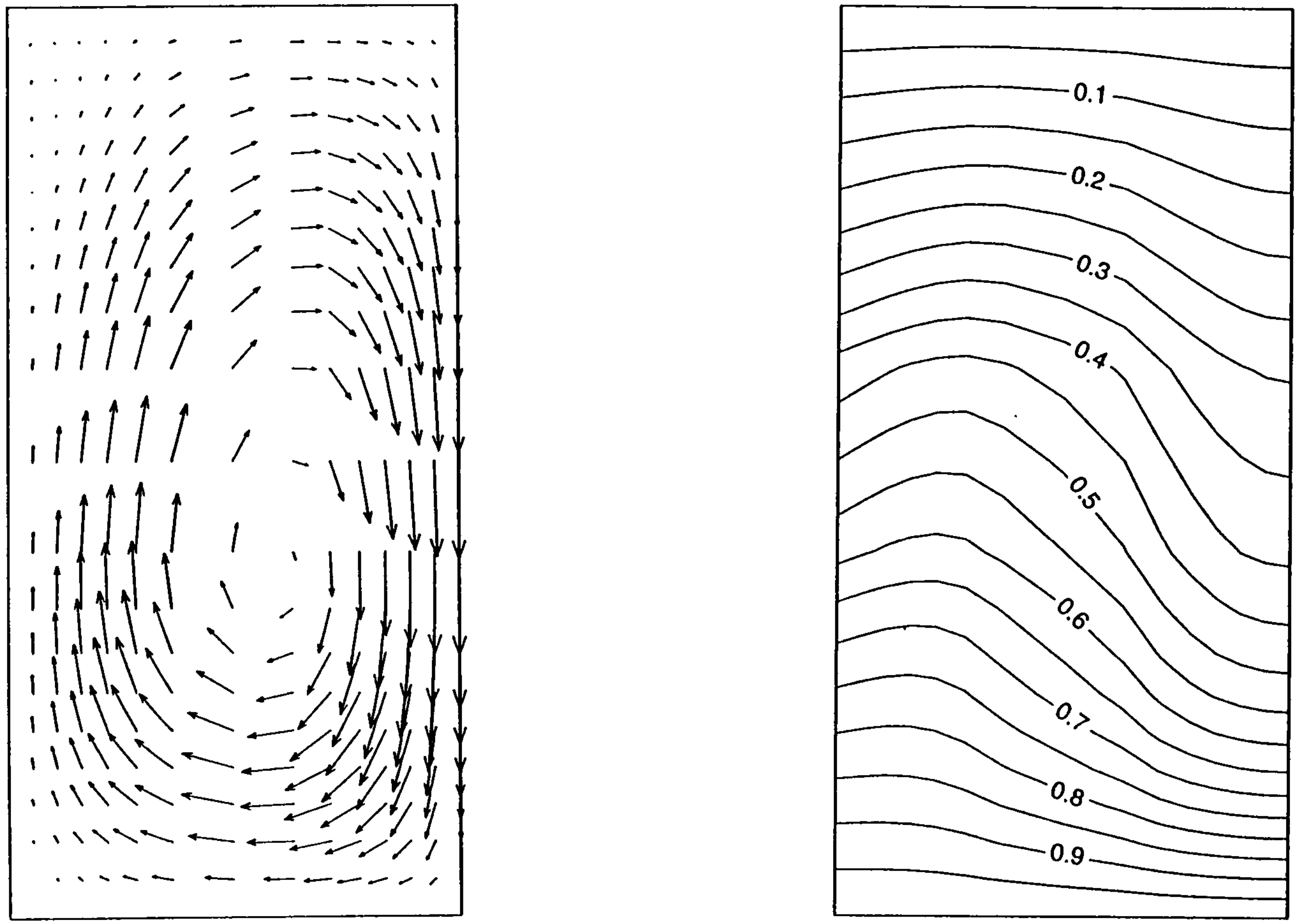

(a) Velocity vector plot

(b) Isotherms

Figure 3.14 Velocity vector plot and isotherms for Case III (AR=2.0, Ncr=1.5, Gr=2000)

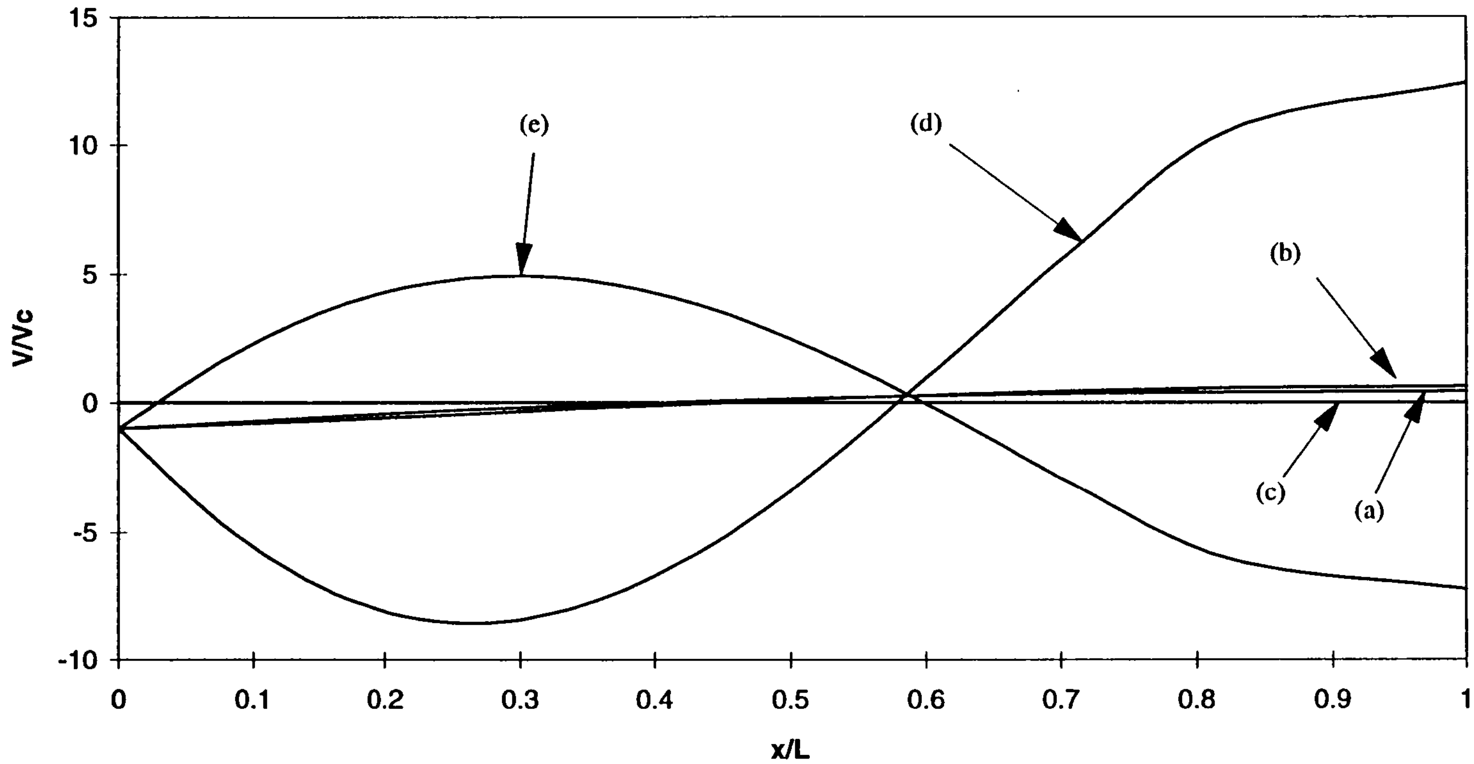

Figure 3.15 The normalized vertical velocity component at the center horizontal plane (Case III). (a) Gr=0; (b) Gr=375; (c) Gr=375 when C_S=0; (d) Gr=1598; (e) Gr=1601

problem. However, the flow isotherms are significantly altered near the critical Grashof number because of the strong circulation and a conduction region appears only near the horizontal walls (see Figure 3.12 and 3.13). Since the largest velocity occurs at the axis of symmetry, the isotherms near the axis are affected the most.

Figures 3.16 (a), (b) and Table 3.1 show the average Nusselt number at the lower wall as a function of Grashof number. Below the critical Grashof number (around Gr=1600 for AR=2 and N_{CR}=1.5), the flow is dominated by conduction and the difference of the average Nusselt number on the bottom wall from 1 is observed to be at most 7%. In the counterclockwise circulation observed at pre-critical values of Grashof number, the cold flow driven by thermal creep from the top is heated by the left wall. When the flow reaches the bottom wall, the temperature difference between the fluid and the wall is less than that observed for the corresponding pure conduction problem and the average Nusselt number on the bottom wall is less than 1. The Nusselt number increases as Grashof number increases for Grashof number larger than the critical value and the flow begins to be influenced by buoyancy in a significant way. In the clockwise circulation for this range of Grashof number, the cold flow is first heated by the bottom wall before it is cooled by the left and the top walls. As clockwise flow strength increases, more heat is removed from the bottom wall and average Nusselt number exceeds 1. Therefore, it is noted that the direction of flow circulation as established by thermal creep or buoyancy ultimately determines the direction of heat flux at the left wall.

The average Nusselt number at the bottom wall slowly decreases as Grashof number inncreases for Grashof numbers less than 1300 because the strength of flow approaching the bottom wall increases. However, in the transition region between Gr=1300 and 1610 the Nusselt number is observed to slowly increase as Grashof number increases. The exact average Nusselt number at the critical Grashof number is difficult to obtain because the

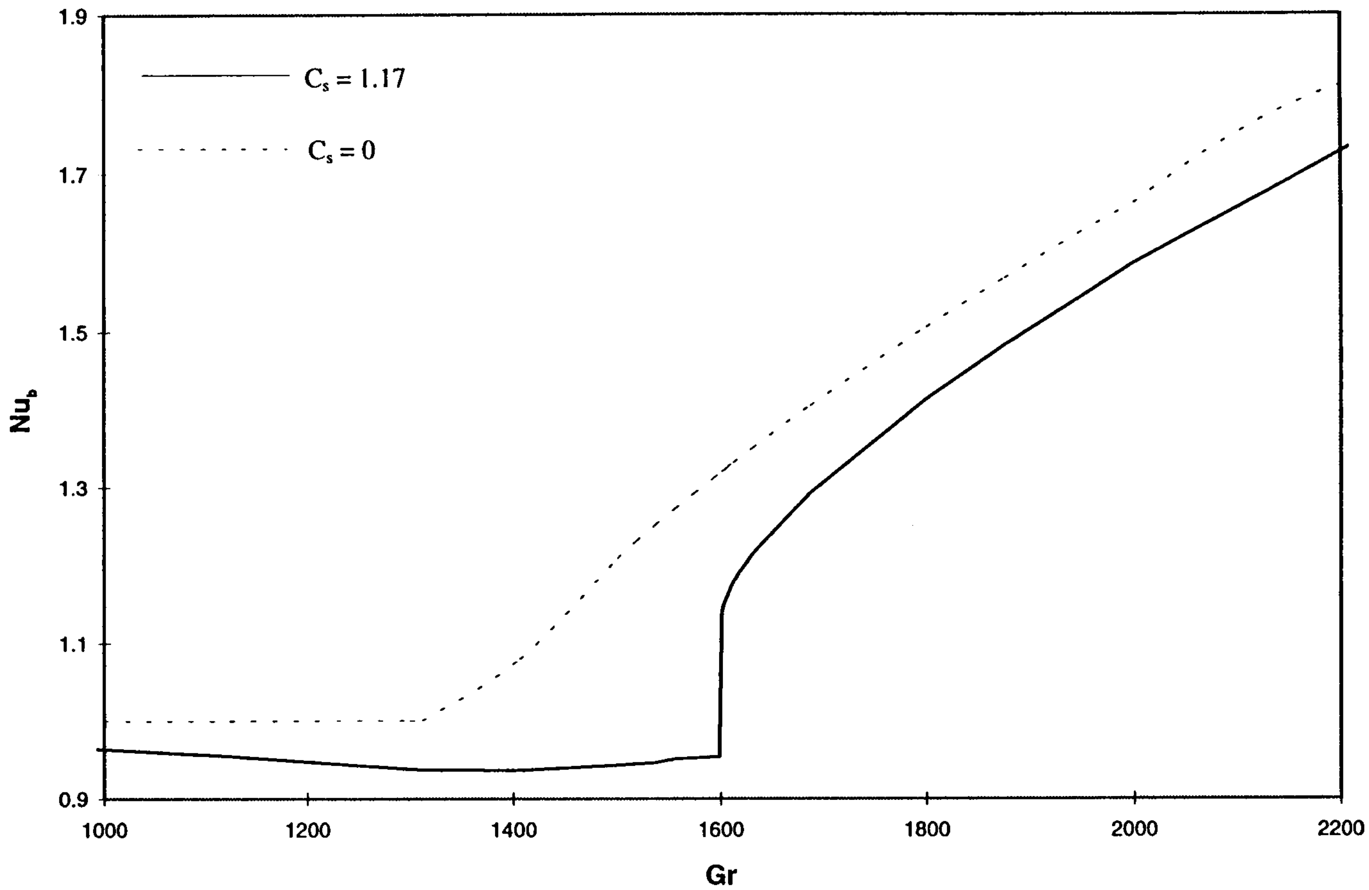

(a) Variation of Nusselt number with Grashof number (1<Gr<5000)

Figure 3.16 Variations of Nusselt number at the bottom wall for Case III.

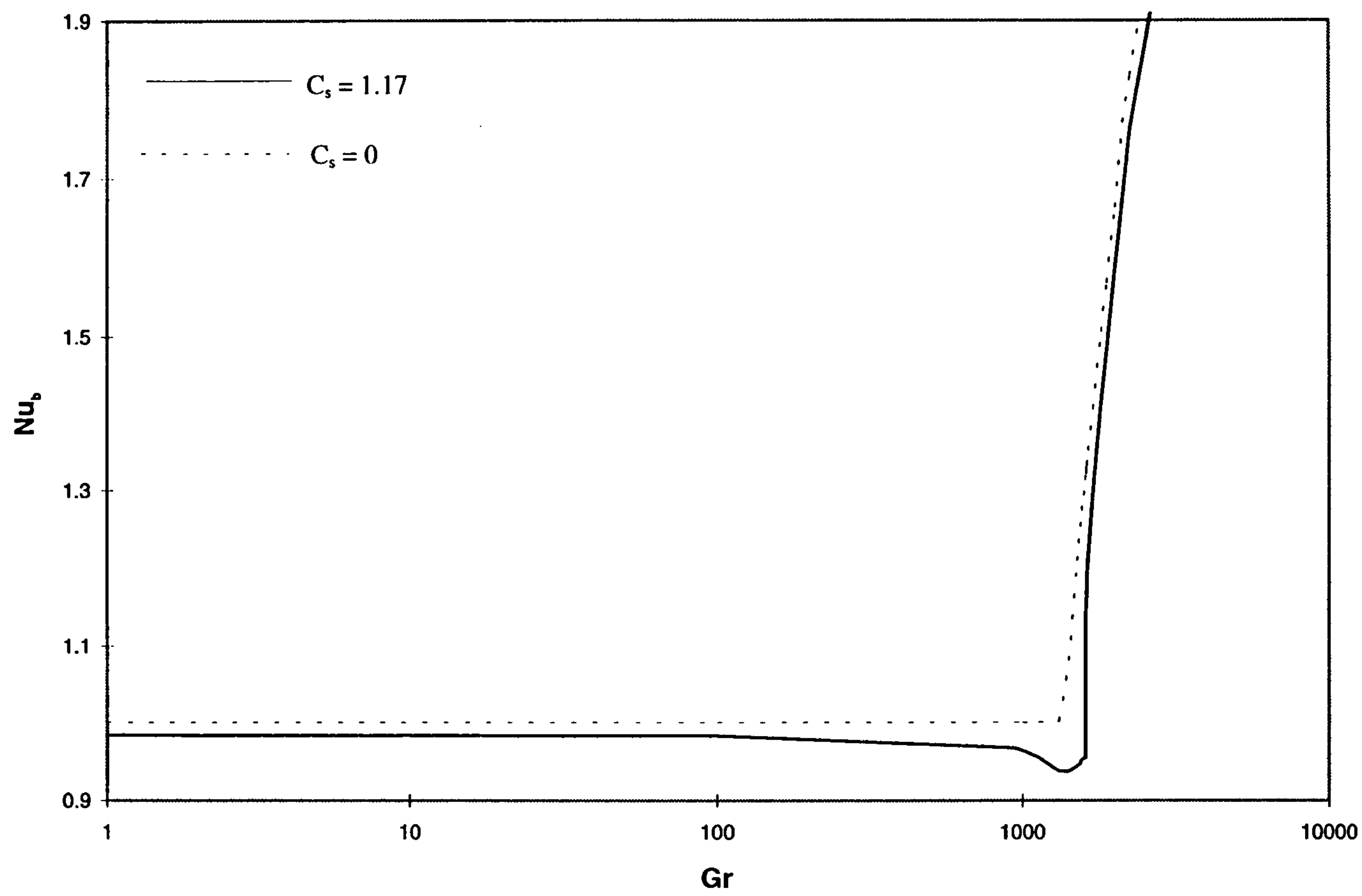

(b) Variation of Nusselt number with Grashof number (close up for values between Gr=1000 and 2200)

Figure 3.16 (continued)

Table 3.1 The variation of Nusselt number at the bottom wall with Grashof number for Case III

Gr	$Nu_b(C_s=1.17)$	$Nu_b(C_s=1.17)$
0	0.984	1.000
100	0.983	1.000
1000	0.964	1.000
1300	0.939	1.001
1500	0.943	1.209
1601	1.140	1.320
1800	1.414	1.506
2000	1.587	1.664
5000	2.504	2.565

solution converges with difficulty near that point. The Nusselt number at the critical Grashof number does rapidly increase at and beyond the critical Grashof number as also observed in Figure 3.16 (b).

For comparison purposes, the results which exclude thermal creep boundary condition are presented together with those including creep in Figure 3.16. In this case, the same trend is observed with the noted exception that the instability near the critical Grashof number is absent and there is a smooth transition from the conduction- to convection-dominated region. Therefore, this unstable behavior of the flow near the critical Grashof number, which is present due to thermal creep, should be carefully taken into account in the flow analysis under microgravity condition.

3.4 The Effect of the Orientation of the Enclosure Geometry

To investigate the effect of the orientation of the enclosure in Case III (AR=2.0 and N_{CR}=1.5), three different gravity vector directions were considered: positive y-direction, negative x-direction and positive x-direction. For easy comparison of different cases only the direction of gravity vector was changed and its magnitude was kept constant. The negative y-direction gravity has already been discussed and presented as Case III.

For the case in which gravity vector is directed toward the positive y-direction, the fluid is stable. The flow is dominated by thermal creep and the counterclockwise flow rotation is shown in Figure 3.17 for Gr_X=0 and Gr_y=-375. The contribution of convection to the heat transfer is minor and heat conduction remains primary as shown by isotherms in Figure 3.17. The isotherms indicated a stratified flow indicating conduction heat transfer in the vertical direction to be dominant. The flow is observed to be weak as compared to other gravity vector orientation as shown in Figure 3.18.

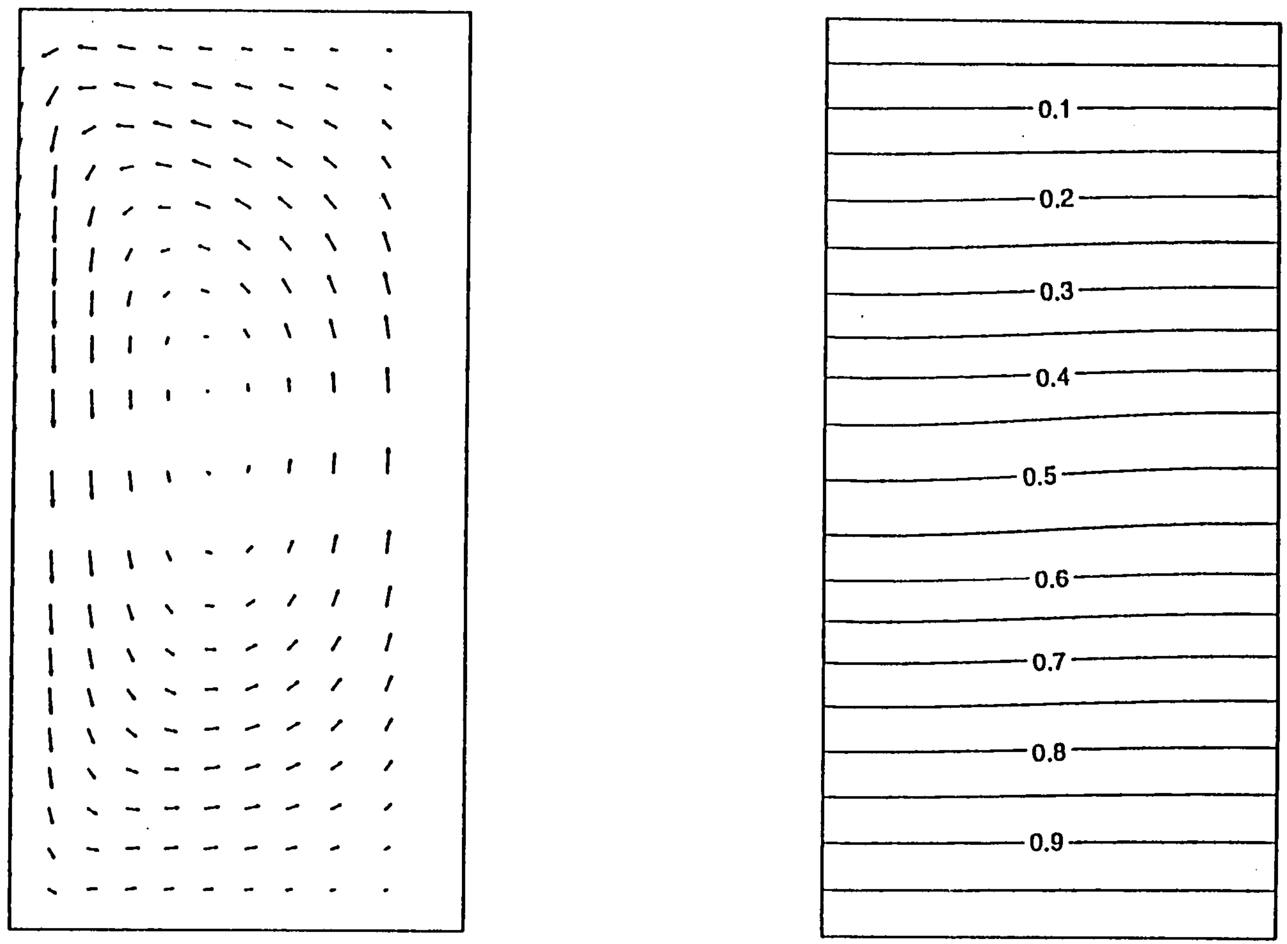

(a) Velocity vector plot

(b) Isotherms

Figure 3.17 Velocity vector plot and isotherms for Case IV (AR=2.0, Ncr=1.5, Gr_x=0, Gr_y=-375)

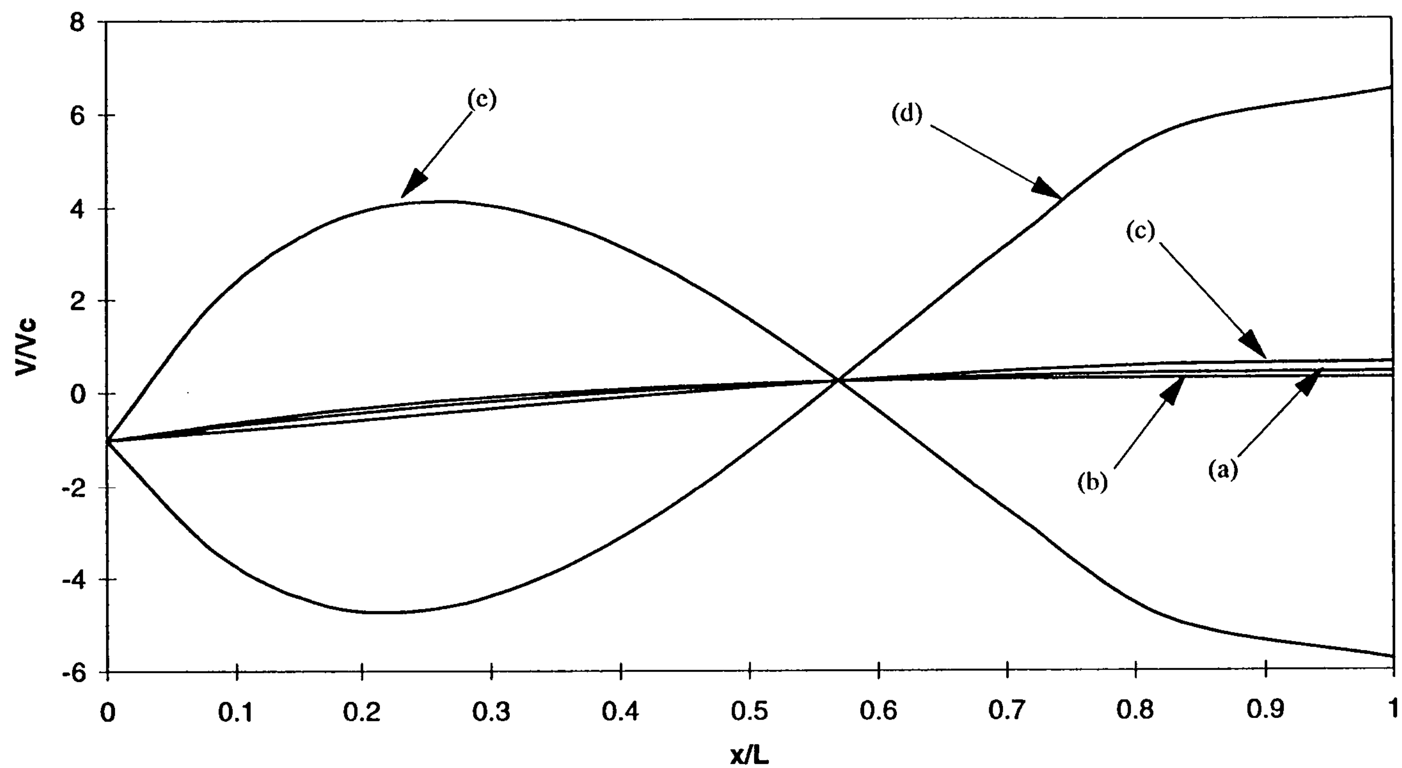

Figure 3.18 The normalized vertical velocity component at the center horizontal plane (Case IV).
(a) $Gr_x = 0$ and $Gr_y = 0$; (b) $Gr_x = 0$ and $Gr_y = 375$; (c) $Gr_x = 0$ and $Gr_y = -375$; (d) $Gr_x = 375$ and $Gr_y = 0$; (e) $Gr_x = -375$ and $Gr_y = 0$

If the direction of gravity is in the positive x-direction, the buoyancy force drives the flow clockwise. Figure 3.19 shows the flow direction in this case. The flow generated by buoyancy force is strong enough to overwhelm the thermal creep flow and contribute to the transfer of heat. The isotherms are shifted upward near the right symmetric axis, and downward near the left wall. The largest axial velocity is 5.5 times bigger than thermal creep velocity as shown in Figure 3.18.

The flow behavior is similar when the gravity vector is in the negative x-direction, except flow rotation of flow is in the opposite direction as shown in Figure 3.20. The resulting velocity field is at most 5% stronger than the previous gravity vector along positive x-direction. This flow enhancement is due to increased buoyancy force in the positive direction near the left wall. Finally it is noted that in microgravity condition the flow remains dominated by the buoyancy force when applied gravity vector is normal to the direction of creep flow.

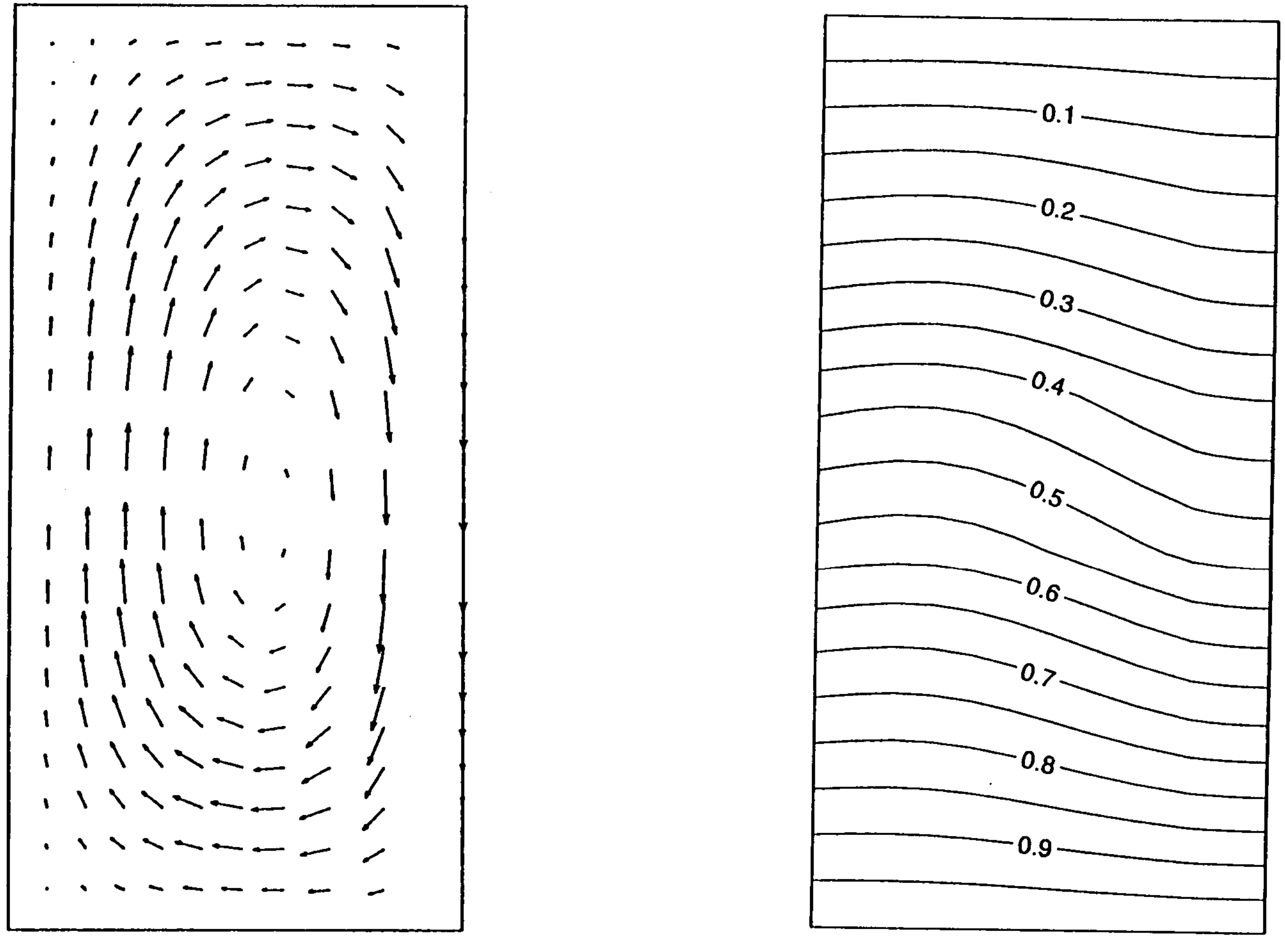

(a) Velocity vector plot

(b) Isotherms

Figure 3.19 Velocity vector plot and isotherms for Case IV (AR=2.0, Ncr=1.5, Gr_x=-375, Gr_y=0)

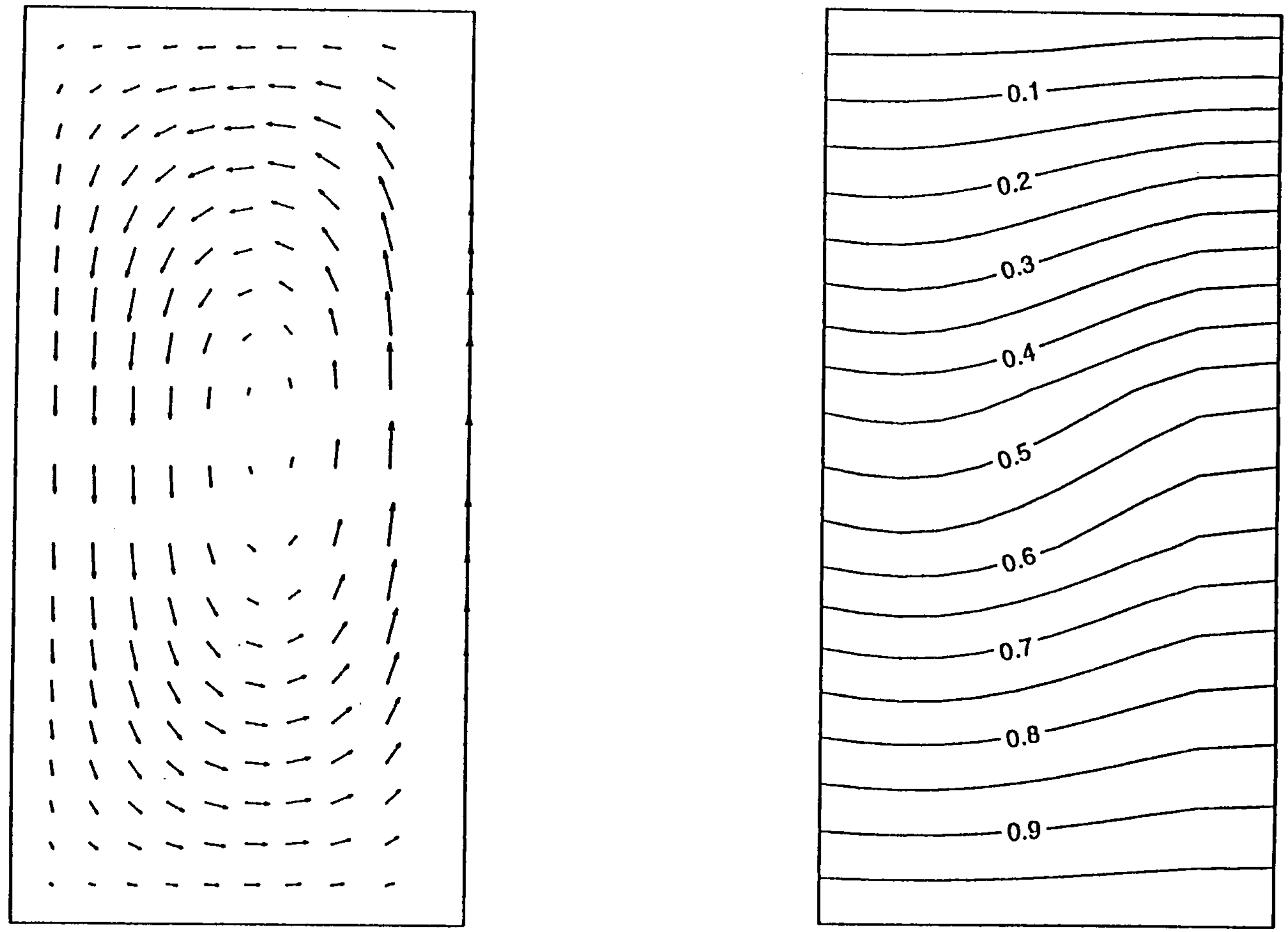

(a) Velocity vector plot (b) Isotherms

Figure 3.20 Velocity vector plot and isotherms for Case IV (AR=2.0, Ncr=1.5, Gr_x=375, Gr_y=0)

Chapter 4
SUMMARY AND CONCLUSIONS

In this study it is shown that, contrary to common assumption, significant flow may be generated due to the presence of thermal creep even under zero-gravity condition. Furthermore, it is found that thermal creep induced by a nonisothermal wall may significantly alter the assumed behavior of enclosed fluids due to its interaction with buoyancy in microgravity environment. Also, thermal creep and buoyancy can provide a complicated flow pattern and instability under certain critical conditions. For example, the result for heating from the sidewalls showed complicated cell circulation and heating from the below showed that the flow can become unstable near critical value of Grashof number. For large Grashof number, the effect of thermal creep remains very limited to the region near the creep-inducing wall as expected.

Despite the great deal of contribution of thermal creep to the flow pattern, heat transfer remains dominated by conduction in most of the cases. A noted exception is near the critical Grashof number in Case III where sudden change and flow instability are observed and convective heat transfer may become important relative to conduction. For Grashof number exceeding the critical value, heat transfer is dominated by convection due to buoyancy.

The contribution of thermal creep also depends on the direction of gravity vector. When thermal creep velocity direction is normal to the gravity vector, the flow is observed to be dominated by buoyancy force as shown in Case IV. Also, flow velocity is higher in this case relative to the condition in which creep velocity is parallel to the gravity vector. Therefore, a change of direction of gravity vector, for example encountered under microgravity conditions with g-jitter, may produce important flow behavior that requires a detailed and more careful analysis. Only then an accurate estimate of fluid velocity and temperature will be possible in such delicate applications as crystal growing and manufacturing under space microgravity conditions.

REFERENCES

REFERENCES

[1] Everitt, C.W.F., *James Clerk Maxwell: Physicist and Natural Philosopher*, Charles Scribner's Sons, New York, 1975, pp. 156-160

[2] Kennard, E. H., *Kinetic Theory of Gases*, McGraw-Hill, New York, 1938, pp. 327-330.

[3] Nadarajah, A., Rosenberger, F., and Alexander, I. D., "Effects of Buoyancy-driven Flow and Thermal Boundary Conditions on Physical Vapor Transport," *Journal of Crystal Growth*, Vol. 118, 1992, pp. 49-52

[4] Talbot, L., Cheng, R. K., Schefer, R. W., and Willis, D. R., "Thermophoresis of Particles in a Heated Boundary Layer," *Journal of Fluid Mechanics*, Vol. 101, Pt. 4, 1980, pp. 737-758

[5] Rosner, D. E., "Sidewall Gas 'Creep' and 'Thermal Stress Convection' in Microgravity Experiments on Film Growth by Vapor Transport," *Physics of Fluids*, Vol. A1, No. 11, 1989, pp. 1761-1763.

[6] Rosner, D. E. and Keyes, D. E., "Theoretical Studies in Support of the 3M-Vapor Transport(PVTOS-) Experiment," NASA Report No. CR 185122, 1989.

[7] Vedha-Nayagam, M. and Mackowski, D. W., "Effect of Thermal Creep on Buoyancy-Induced Flows in Low-Gravity," *Journal of Thermophysics and Heat Transfer*, Vol. 6, No. 4, 1992, pp. 753-755

[8] Walker, D. G., Mackowski, D. W., and Knight, R. W., "The Effect of Thermal Creep on Physical Vapor Transport in Microgravity," AIAA 94-0567, 1994

[9] Patankar, S. V., *Numerical Heat Transfer and Fluid Flow*, Hemisphere Publishing Corp., 1980

APPENDICES

Appendix A

Discretization Procedure

The generalized conservation Equation (2.7) can be written as

$$\frac{\partial}{\partial t}(\rho\phi)+\frac{\partial J_x}{\partial x}+\frac{\partial J_y}{\partial y}=S$$

(A.1)

where J_x and J_y are the total fluxes defined by

$$J_x \equiv \rho u\phi-\Gamma\frac{\partial\phi}{\partial x}$$

$$J_y \equiv \rho v\phi-\Gamma\frac{\partial\phi}{\partial y}$$

By performing integration of Equation (A.1) over the control volume as shown in Figure A.1, the governing equation becomes:

$$\frac{\left(\rho_P\phi_P-\rho_P^\circ\phi_P^\circ\right)\Delta x\Delta y}{\Delta t}+J_e-J_w+J_n-J_s=\left(S_C+S_P\phi_P\right)\Delta x\Delta y$$

(A.2)

where the source term is linearized and ° denotes the values at the previous time step. The fully implicit scheme is used for all variables. The quantities J_e, J_w, J_n, and J_s are the integrated total fluxes over the control-volume surfaces.

Similarly, the unsteady continuity equation can be integrated over the control volume to obtain:

$$\frac{\left(\rho_P-\rho_P^\circ\right)\Delta x\Delta y}{\Delta t}+F_e-F_w+F_n-F_s=\left(S_C+S_P\phi_P\right)\Delta x\Delta y$$

(A.3)

where F_e, F_w, F_n, and F_s are the mass flow rates through the control-volume faces and the definitions of the symbols are given in Equation (2.8).

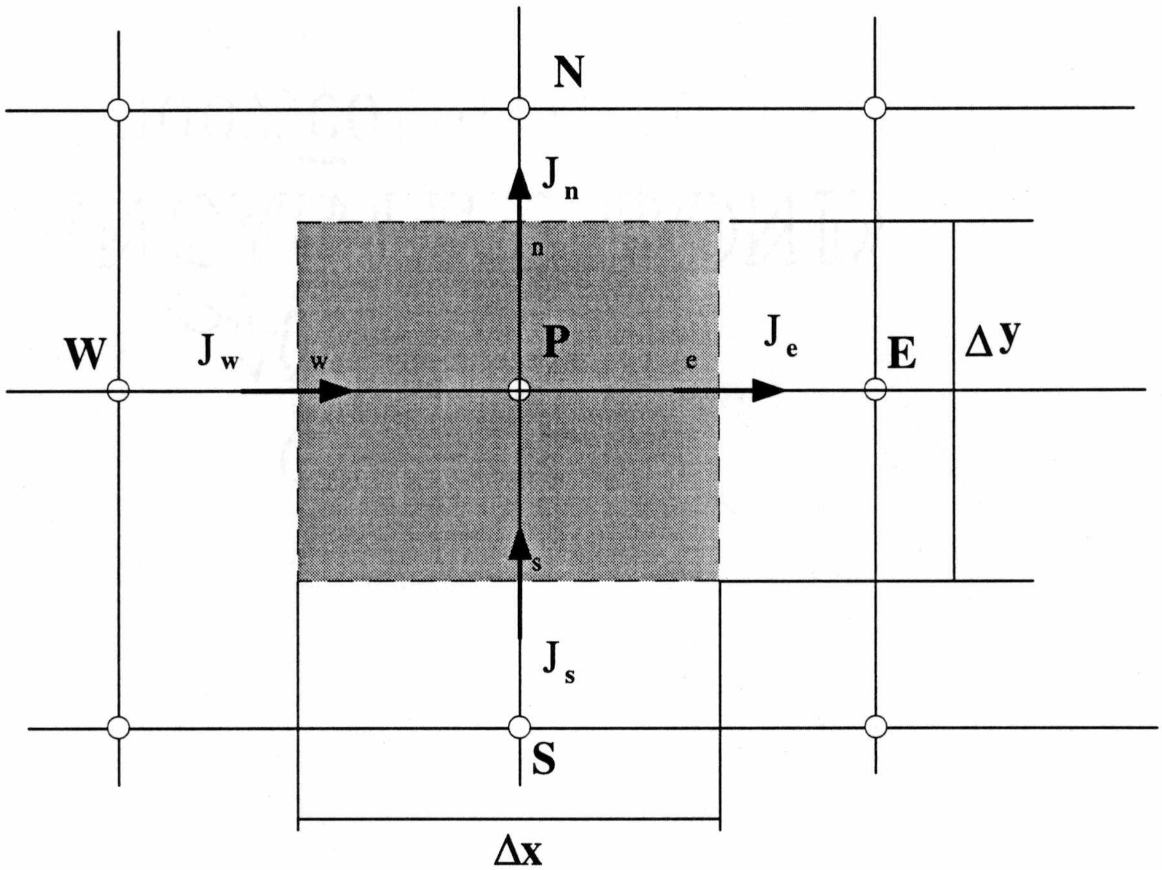

Figure A.1. Main control volume

Multiplying Equation (A.3) by ϕ_P and subtracting it from Equation (A.2) gives:

$$\left(\phi_P-\phi_P^\circ\right)\frac{\rho_P^\circ\Delta x\Delta y}{\Delta t}+\left(J_e-F_e\phi_P\right)-\left(J_w-F_w\phi_P\right)+\left(J_n-F_n\phi_P\right)$$
$$-\left(J_s-F_s\phi_P\right)=\left(S_C+S_P\phi_P\right)\Delta x\Delta y$$

(A.4)

Assuming the uniformity over a control-volume face, the terms such as $J_e-F_e\phi_P$ and $J_w-F_w\phi_P$ can expressed in the following form

$$J_e-F_e\phi_P=a_E\left(\phi_P-\phi_E\right)$$
$$J_w-F_w\phi_P=a_W\left(\phi_W-\phi_P\right)$$

where

$$a_E=D_eA(|P_e|)+max\left(-F_e,0\right)$$
$$a_W=D_wA(|P_w|)+max\left(F_w,0\right)$$

The definition of D is given Equation (2.8) and function A can be chosen from the Table A.1. Similar expressions can be applied to $J_n-F_n\phi_P$ and $J_s-F_s\phi_P$,. Substituting the four expressions into Equation (A.4) and reorganizing the terms, results in the discretized Equation (2.8).

Table A.1 The function of A(|P|) for different schemes

Scheme	Formula for A(|P|)
Central difference	$1-.5\|P\|$
Upwind	1
Hybrid	[0,1-0.5|P|]
Power law	[0,(1-0.1|P|)^5]
Exponential	|P|/(exp(|P|)-1)

Appendix B
CODE

Main Program: NCRC.FOR

```
*     A Program to anlayze the convection
*     of a fluid in a rectangular enclosure with thermal creep flow.
*     Nondimensional variables are used.

*     Declaration of varaibles
          INCLUDE 'gridnu.f'
          REAL UO(0:N+1,0:M+1),VO(0:N+1,0:M+1)
          REAL U(0:N+1,0:M+1),V(0:N+1,0:M+1)
          REAL T(0:N+1,0:M+1),TO(0:N+1,0:M+1),TT(0:N+1,0:M+1)
          REAL PS(0:N+1,0:M+1),PO(0:N+1,0:M+1)
          REAL UA(N,M,4),UP(N,M),UB(N,M),UBO(N,M)
          REAL VA(N,M,4),VP(N,M),VB(N,M),VBO(N,M)
          REAL PA(N,M,4),PP(N,M),PB(N,M)
          REAL TA(N,M,4),TP(N,M),TB(N,M),TBO(N,M)
          REAL B(N,M),GROS(6),AR(5),NDT(5)
          REAL ASPR,DX,H,GRAVITY,DTEMP,DVISC,PR,BETA
          COMMON U,V,T
          COMMON PR,DELX,DELY,GR,APO

          DATA GROS/0./
          DATA AR/2./

*     VARIABLES LIST ---------------------------
*     U,V : VELOCITY COMPONENTS
*     UO,VO : OLD VALUES OF U AND V
*     T,TO : TEMPERATURE AND ITS OLD VALUE
*     PS : P* ( PRESSURE )
*     PO : P' ( PRESSURE )
*     GRO : Gravity Constant
*     GR : Grashof Number
*     ASPR : Aspect Ratio = H/L
*     CRN : Ncr
*     PR : Prandtl Number
*     DELX, DELY, DELT : Grid Sizes of x, y-direction and time
*     TOL, CTOL : Convergence Tolerance

*     Input Data ----------------------------------
          OPEN(3,FILE = 'conc.dat', STATUS = 'old' )
            READ(3,*) GRO,ASPR,CRN,PR
            READ(3,*) TOL,CTOL,DELT
          CLOSE(3)

*     Constants Calculation ------------------------
          CS = 1.17  !* Cs
          GR = GRO*CRN/(ASPR**3)  !* Grashof Number
          Time = 0.

*     Grid Sizes and Coeff. for Unsteady term ---------
          DELX = 1./REAL(N)
          DELY = ASPR/REAL(M)
          APO=DELX*DELY/DELT

*     Guessed Velocities, Temperature, and Density
*
          DO J = 1, N
           U(0,J) = 0.              !* Left Wall
           V(0,J) = -CS/ASPR*CRN/(CRN*(1-DELY*J/ASPR)+1)
           T(0,J) = 1.-(DELY*(J-.5))/ASPR
           U(M+1,J) = 0.            !* Right Wall
           V(M+1,J) = 0.
           T(M+1,J) = 0.

          DO I = 1,M
            U(I,J) = 0.             !* Main Body
            V(I,J) = 0.
            T(I,J) = 0.
            PO(I,J) = 0.
            PS(I,J) = 0.
           END DO
          END DO

          DO I=0,M+1                !* Bottom and Top Walls
           U(I,0) = 0.
           U(I,N+1) = 0.
           V(I,0) = 0.
           V(I,N+1) = 0.
           T(I,0) = 1.
           T(I,N+1) = 0.
          END DO

          CALL SHIFT(UO,U)
          CALL SHIFT(VO,V)
          CALL SHIFT(TT,T)
          CALL SHIFT(TO,T)

          DT = 1.

          DO WHILE((DT.GT.TOL).AND.(Time.LT.5000.))
* Time Advanced--------------------------------
          Time = Time + DELT
```

```
      DO J=1,N
       DO I=1,M
        UBO(I,J) = APO * U(I,J)
        VBO(I,J) = APO * V(I,J)
        TBO(I,J) = APO * T(I,J)
       END DO
      END DO

* U Hat and V Hat-----------------------------
100   Continue
      CALL UCOEFF(UP,UA,UB)
      CALL VCOEFF(VP,VA,VB)

      DO J=1,N
       DO I=1,M
        USUM = UA(I,J,1)*UO(I+1,J)+UA(I,J,2)*UO(I-1,J)+
   C UA(I,J,3)*UO(I,J+1)+UA(I,J,4)*UO(I,J-1)+UB(I,J)+UBO(I,J)
        U(I,J) = USUM/UP(I,J)

        VSUM = VA(I,J,1)*VO(I+1,J)+VA(I,J,2)*VO(I-1,J)+
   C VA(I,J,3)*VO(I,J+1)+VA(I,J,4)*VO(I,J-1)+VB(I,J)+VBO(I,J)
        V(I,J) = VSUM/VP(I,J)
       END DO
      END DO

* Pressure Star-----------------------------
      CALL PCOEFF(PP,PA,PB,UP,VP,BMAX)
      CALL TDMA(PS,PP,PA,PB)

* U Star and V Star --------------------------
      DO J=1,N
       DO I=1,M-1
        B(I,J)=UBO(I,J)+UB(I,J)+(PS(I,J)-PS(I+1,J))*DELY
       END DO
       B(M,J)=UBO(M,J)+UB(M,J)
      END DO
      CALL TDMA(U,UP,UA,B)

      DO I=1,M
       DO J=1,N-1
        B(I,J)=VBO(I,J)+VB(I,J)+(PS(I,J)-PS(I,J+1))*DELX
       END DO
       B(I,N)=VBO(I,N)+VB(I,N)
      END DO
       CALL TDMA(V,VP,VA,B)

* Pressure Prime --------------------------
      CALL PCOEFF(PP,PA,PB,UP,VP,BMAX)
      CALL TDMA(PO,PP,PA,PB)

* Correction of U and V --------------------
      DO J=1,N
      DO I=1,M
       IF (I.NE.M) U(I,J)=U(I,J)+(PO(I,J)-PO(I+1,J))*DELY/UP(I,J)
       IF (J.NE.N) V(I,J)=V(I,J)+(PO(I,J)-PO(I,J+1))*DELX/VP(I,J)
      END DO
      END DO
      CALL PCOEFF(PP,PA,PB,UP,VP,BMAX)
      CALL SHIFT(UO,U)
      CALL SHIFT(VO,V)

* Calculation of Temperature -----------------
99    CALL TCOEFF(TP,TA,TB)
      DO J=1,N
       DO I=1,M
        B(I,J) = TBO(I,J) + TB(I,J)
       END DO
      END DO
      CALL TDMA(T,TP,TA,B)

* Convergency --------------------------------
      BTM = 0.
      DO J=1,N
      DO I=1,M
       IF (TO(I,J).EQ.0.) THEN
        BTM = AMAX1(BTM,ABS(TO(I,J)-T(I,J)))
       ELSE
        BTM = AMAX1(BTM,ABS((TO(I,J)-T(I,J))/TO(I,J)))
       END IF
      END DO
      END DO
      CALL SHIFT(TO,T)

      IF ((BTM.GT.CTOL).or.(BMAX.GT.CTOL)) GOTO 100

103   PRINT*,'END OF TIME=',Time


* Convergent to Steady Solution --------------
      DT = 0.
      DO J=1,N
       DO I=1,M
```

```
     IF (TT(I,J).EQ.0.) THEN
      DER = ABS(T(I,J)-TT(I,J))
     ELSE
      DER = ABS((T(I,J)-TT(I,J))/TT(I,J))
     END IF
     DT = AMAX1(DT,DER)
    END DO
   END DO
   CALL SHIFT(TT,T)
   END DO        !* WHILE LOOP

   PRINT*,AVNUL(ASPR),',',AVNUH(ASPR,0),',',AVNUH(ASPR,N+1)
   CALL OUTPUT(IDEN,0)
   STOP
   END


*Subroutines for the coefficients in discretized eqns.--------
*Coefficients in X-dir momentum equation--------------------
   SUBROUTINE UCOEFF(UP,UA,UB)
   INCLUDE 'gridnu.f'
   REAL U(0:M+1,0:N+1),V(0:M+1,0:N+1),T(0:M+1,0:N+1)
   REAL UA(M,N,4),UP(M,N),UB(M,N)
   INTEGER I,J
   COMMON U,V,T
   COMMON PR,DELX,DELY,GR,APO

   DO J=1,N              !* Right Wall
    DO K=1,4
     UA(M,J,K) = 0.
    END DO
    UP(M,J) = 1.
    UB(M,J) = 0.
   END DO

   DO I=1,M-1
    DO J=1,N
     DE = DELY/DELX
     FE = (U(I+1,J)+U(I,J))/2.*DELY
     DW = DE
     FW = (U(I,J)+U(I-1,J))/2.*DELY
    IF (J.EQ.N) THEN
     DN = DELX/DELY*2
    ELSE
     DN = DELX/DELY
    END IF
     FN = (V(I+1,J)+V(I,J))/2.*DELX
    IF (J.EQ.1) THEN
     DS = DELX/DELY*2
    ELSE
     DS = DELX/DELY
    END IF
    FS = (V(I+1,J-1)+V(I,J-1))/2.*DELX

    PE = FE / DE
    UA(I,J,1) = DE * A(ABS(PE)) + AMAX1(-1*FE,0.)
    PW = FW / DW
    UA(I,J,2) = DW * A(ABS(PW)) + AMAX1(FW,0.)
    PN = FN / DN
    UA(I,J,3) = DN * A(ABS(PN)) + AMAX1(-1*FN,0.)
    PSS = FS / DS
    UA(I,J,4) = DS * A(ABS(PSS)) + AMAX1(FS,0.)
    UP(I,J) = APO
     DO K=1,4
      UP(I,J) = UP(I,J) + UA(I,J,K)
     END DO
    UB(I,J) = 0.
    IF (J.EQ.1) THEN
     UB(I,J) = UB(I,J) + UA(I,J,4) * 0.
     UA(I,J,4) = 0.
    END IF
    IF (J.EQ.N) THEN
     UB(I,J) = UB(I,J) + UA(I,J,3) * 0.
     UA(I,J,3) = 0.
    END IF
    IF (I.EQ.1) THEN
     UB(I,J) = UB(I,J) + UA(I,J,2) * 0.
     UA(I,J,2) = 0.
    END IF
    END DO
   END DO
   RETURN
   END


*Coefficients in Y-dir momentum equation--------------------
   SUBROUTINE VCOEFF(VP,VA,VB)
   INCLUDE 'gridnu.f'
   REAL U(0:M+1,0:N+1),V(0:M+1,0:N+1),T(0:M+1,0:N+1)
   REAL VA(M,N,4),VP(M,N),VB(M,N)
   INTEGER I,J
```

```
      COMMON U,V,T
      COMMON PR,DELX,DELY,GR,APO

      DO I=1,M                  !* Top Wall
       VP(I,N) = 1.
       DO K=1,4
        VA(I,N,K) = 0.
       END DO
       VB(I,N) = 0.
      END DO

      DO J=1,N-1
       DO I=1,M
        IF (I.EQ.M) THEN
         DE = DELY/DELX*2
        ELSE
         DE = DELY/DELX
        END IF
        FE = (U(I,J)+U(I,J+1))/2.*DELY

        IF (I.EQ.1) THEN
         DW = DELY/DELX*2
        ELSE
         DW = DELY/DELX
        END IF
        FW = (U(I-1,J)+U(I-1,J+1))/2.*DELY

        DN = DELX/DELY
        FN = (V(I,J)+V(I,J+1))/2.*DELX
        DS = DN
        FS = (V(I,J-1)+V(I,J))/2.*DELX

        PE = FE / DE
        VA(I,J,1) = DE * A(ABS(PE)) + AMAX1(-1*FE,0.)
        PW = FW / DW
        VA(I,J,2) = DW * A(ABS(PW)) + AMAX1(FW,0.)
        PN = FN / DN
        VA(I,J,3) = DN * A(ABS(PN)) + AMAX1(-1*FN,0.)
        PSS = FS / DS
        VA(I,J,4) = DS * A(ABS(PSS)) + AMAX1(FS,0.)
        VP(I,J) = APO
         DO K=1,4
          VP(I,J) = VP(I,J) + VA(I,J,K)
        END DO
        VB(I,J) = GR * (T(I,J)+T(I,J+1))/2.*DELX*DELY

        IF (I.EQ.1) THEN
         VB(I,J) = VB(I,J)+VA(I,J,2)*V(0,J)
         VA(I,J,2) = 0.
        END IF
        IF (I.EQ.M) THEN
         VP(I,J) = VP(I,J)-VA(I,J,1)
         VA(I,J,1) = 0.
        END IF
        IF (J.EQ.1) THEN
         VB(I,J) = VB(I,J)+VA(I,J,4)* 0.
         VA(I,J,4) = 0.
        END IF

        END DO
        END DO

      RETURN
      END

*Coefficient in Energy equation-----------------------------
      SUBROUTINE TCOEFF(TP,TA,TB)
      INCLUDE 'gridnu.f'
      REAL U(0:M+1,0:N+1),V(0:M+1,0:N+1),T(0:M+1,0:N+1)
      REAL TA(M,N,4),TP(M,N),TB(M,N)
      INTEGER I,J
      COMMON U,V,T
      COMMON PR,DELX,DELY,GR,APO

      DO J=1,M
       DO I=1,N
        IF (I.EQ.M) THEN
          DE = 1/PR*DELY/DELX*2
        ELSE
         DE = 1/PR*DELY/DELX
        END IF
        FE = U(I,J)*DELY
        IF (I.EQ.1) THEN
         DW = 1/PR*DELY/DELX*2
        ELSE
         DW = 1/PR*DELY/DELX
        END IF
        FW = U(I-1,J)*DELY
        IF (J.EQ.N) THEN
         DN = 1/PR*DELX/DELY*2
        ELSE
```

```
      DN = 1/PR*DELX/DELY
     END IF
     FN = V(I,J)*DELX
     IF (J.EQ.1) THEN
      DS = 1/PR*DELX/DELY*2
     ELSE
      DS = 1/PR*DELX/DELY
     END IF
     FS = V(I,J-1)*DELX

     PE = FE/DE
     TA(I,J,1) = DE * A(ABS(PE)) + AMAX1(-1*FE,0.)
     PW = FW / DW
     TA(I,J,2) = DW * A(ABS(PW)) + AMAX1(FW,0.)
     PN = FN /DN
     TA(I,J,3) = DN * A(ABS(PN)) + AMAX1(-1*FN,0.)
     PSS = FS / DS
     TA(I,J,4) = DS * A(ABS(PSS)) + AMAX1(FS,0.)
     TP(I,J) = APO
      DO K=1,4
       TP(I,J) = TP(I,J)+TA(I,J,K)
      END DO
     TB(I,J) = 0.

     IF (I.EQ.1) THEN
      TB(I,J) = TB(I,J)+TA(I,J,2)*T(0,J)
      TA(I,J,2) = 0.
     END IF
     IF (I.EQ.M) THEN
      TP(I,J) = TP(I,J) - TA(I,J,1)
      TA(I,J,1) = 0.
     END IF
     IF (J.EQ.1) THEN
      TB(I,J) = TB(I,J)+TA(I,J,4)*T(I,0)
      TA(I,J,4) = 0.
     END IF
     IF (J.EQ.N) THEN
      TB(I,J) = TB(I,J)+TA(I,J,3)*T(I,M+1)
      TA(I,J,3) = 0.
     END IF

    END DO
    END DO

    RETURN
    END

C----------------------------------------------------
      SUBROUTINE PCOEFF(PP,PA,PB,UP,VP,BMAX)
      INCLUDE 'gridnu.f'
      REAL U(0:M+1,0:N+1),V(0:M+1,0:N+1),T(0:M+1,0:N+1)
      REAL PA(M,N,4),PP(M,N),PB(M,N)
      REAL UP(M,N),VP(M,N)
      INTEGER I,J
      COMMON U,V,T
      COMMON PR,DELX,DELY,GR,APO
      BMAX = 0.
      DO J=1,N
      DO I=1,M
      IF (I.EQ.M) THEN
       PA(I,J,1) = 0.
      ELSE
       PA(I,J,1) = DELY**2 / UP(I,J)
      END IF
      IF (J.EQ.N) THEN
       PA(I,J,3) = 0.
      ELSE
       PA(I,J,3) = DELX ** 2 / VP(I,J)
      END IF

      IF (J.EQ.1) THEN
       PA(I,J,4) = 0.
      ELSE
       PA(I,J,4) = DELX **2 /VP(I,J-1)
      END IF

      IF (I.EQ.1) THEN
       PA(I,J,2) = 0.
      ELSE
       PA(I,J,2) = DELY **2/UP(I-1,J)
      END IF

      PP(I,J) = 0.
       DO K = 1,4
        PP(I,J) = PP(I,J) + PA(I,J,K)
       END DO
      PB(I,J) = (V(I,J-1) - V(I,J)) * DELX
      PB(I,J) = PB(I,J) + (U(I-1,J) - U(I,J))*DELY
      If (V(I,J).NE.0.) BMAX=AMAX1(BMAX,ABS(PB(I,J)/V(I,J)/DELX))
      If (U(I,J).NE.0.) BMAX=AMAX1(BMAX,ABS(PB(I,J)/U(I,J)/DELY))
       END DO
      END DO
```

```
      RETURN
      END

*Function A(P) -- Power Law -----------------------------
      REAL FUNCTION A(P)
      REAL P
      A = AMAX1(0.,((1-0.1*ABS(P))**5))
      RETURN
      END


*Substituting the new velocity to old variables--------------
      SUBROUTINE SHIFT(A,B)
      INCLUDE 'gridnu.f'
      REAL U(0:M+1,0:N+1),V(0:M+1,0:N+1),T(0:M+1,0:N+1)
      REAL A(0:M+1,0:N+1),B(0:M+1,0:N+1)
      INTEGER I,J
      COMMON U,V,T
      COMMON PR,DELX,DELY,GR,APO
      DO J = 1,N
       DO I = 1,M
        A(I,J) = B(I,J)
       END DO
      END DO
      RETURN
      END


*Subroutine for output file--------------------------------
      SUBROUTINE OUTPUT(IDEN,kk)
      INCLUDE 'gridnu.f'
      REAL U(0:M+1,0:N+1),V(0:M+1,0:N+1),T(0:M+1,0:N+1)
      INTEGER I,J,kk
      CHARACTER NAME*12
      COMMON U,V,T
      COMMON PR,DELX,DELY,GR,APO

c     PRINT*,'OUTPUT FILE :',NAME(IDEN,kk)
      OPEN (4,FILE = NAME(IDEN,kk))
      WRITE(4,*) 'TITLE = "GR =',GR,'"'
      WRITE(4,*) 'VARIABLES = "X","Y","U","V","T"'
      WRITE(4,*)'ZONE F=POINT, I=',N+2,', J=',M+2
      WRITE(4,*) 0,0,0,0,1.
      DO I=1,M
      WRITE(4,*) DELX*(I-.5),0,(U(I,0)+U(I-1,0))/2.,0,T(I,0)
      END DO
      WRITE(4,*) 1,0,0,0,1.
      DO J=1,N
       WRITE(4,*) 0,DELY*(J-.5),0,(V(0,J)+V(0,J-1))/2.,T(0,J)
       DO I =1,N
        WRITE(4,*) DELX*(I-.5),DELY*(J-.5),
C  (U(I,J)+U(I-1,J))/2.,(V(I,J)+V(I,J-1))/2.,T(I,J)
       END DO
       WRITE(4,*) 1,DELY*(J-.5),0,(V(M,J)+V(M,J-1))/2.,T(M,J)
      END DO
      WRITE(4,*) 0,1,0,0,0.
      J=N+1
      DO I=1,M
       WRITE(4,*) DELX*(I-.5),1,(U(I,J)+U(I-1,J))/2.,0,T(I,N+1)
      END DO
      WRITE(4,*) 1,1,0,0,0.
      WRITE(4,*) 'GEOMETRY X=0.,Y=0.,T=RECTANGLE'
      WRITE(4,*) ' 1.0 1.0'

      CLOSE(4)

      return
      end


      SUBROUTINE TDMA(PH,AP,A,B)
      INCLUDE 'gridnu.f'
      REAL P(M),Q(M)
      REAL PH(0:M+1,0:N+1),TM(0:M+1,0:N+1)
      REAL AP(M,N),A(M,N,4),B(M,N)
      REAL D,DIS,TOL,DN,como,COM
      INTEGER I,J,IE,JE

      TOL = 1E-6
      W = .8
      COMO = 0.
1000  do kk=1,10
      DO J = 1,N
       D = A(1,J,3)*PH(1,J+1)+A(1,J,4)*PH(1,J-1)+B(1,J)
       P(1) = A(1,J,1)/AP(1,J)
       Q(1) = D/AP(1,J)
       DO I = 2,M
        D = A(I,J,3)*PH(I,J+1)+A(I,J,4)*PH(I,J-1)+B(I,J)
        DN = AP(I,J)-A(I,J,2)*P(I-1)
        P(I) = A(I,J,1)/DN
        Q(I) = (D+A(I,J,2)*Q(I-1))/DN
       END DO
```

```
        TM(M,J) = Q(M)

        DO I = M-1,1,-1
         TM(I,J) = P(I) * TM(I+1,J) + Q(I)
        END DO

        DO I=1,M
         PH(I,J) = PH(I,J) + W*(TM(I,J)-PH(I,J))
        END DO
        END DO
        end do

         COM = 0.

         DO J=1,N
          DO I=1,M
           SUM = A(I,J,1)*PH(I+1,J)+A(I,J,2)*PH(I-1,J)+A(I,J,3)
C  *PH(I,J+1)+A(I,J,4)*PH(I,J-1)+B(I,J)
           DIS = SUM/AP(I,J) - PH(I,J)
           If (ABS(DIS).GT.COM ) THEN
            IE = I
            JE = J
           END IF
           If (PH(I,J) .NE. 0.) Then
            COM = AMAX1(COM,ABS(DIS/PH(I,J)))
           else
            COM = AMAX1(COM,ABS(DIS))
           end if
          END DO
         END DO

        IF (COM.GT.TOL) GOTO 1000

2000    RETURN
        END

        CHARACTER*12 FUNCTION NAME(IDEN,k)
        CHARACTER PRO,ASCII
        INTEGER X,D(4),I,IDEN,k
        X = IDEN
        DO I=1,4
         D(I) = INT(X/(10**(4-I)))
         X = INT(X - D(I)*10**(4-I))
        END DO
        PRO='n'
        NAME = PRO//ASCII(k)//ASCII(D(1))//ASCII(D(2))
c  //ASCII(D(3))//ASCII(D(4))//'.dat'
        RETURN
        END


        CHARACTER FUNCTION ASCII(X)
        INTEGER X
        ASCII=CHAR(X+48)
        RETURN
        END

        REAL FUNCTION AVNUL(ASPR)          !* Nu at the sidewall
        INCLUDE 'gridnu.f'
        REAL U(0:M+1,0:N+1),V(0:M+1,0:N+1),T(0:M+1,0:N+1)
        INTEGER J
        COMMON U,V,T
        COMMON PR,DELX,DELY,GR,APO

        AVNUL = 0.
        DO J=1,M
         AVNUL = AVNUL+(T(0,J)-T(1,J))/DELX*2.*DELY/ASPR
        END DO
        RETURN
        END

        REAL FUNCTION AVNUH(ASPR,ID)       !Nu at the top or bottom wall
        INCLUDE 'gridnu.f'
        REAL U(0:M+1,0:N+1),V(0:M+1,0:N+1),T(0:M+1,0:N+1)
        INTEGER I,ID,JT,JB
        COMMON U,V,T
        COMMON PR,DELX,DELY,GR,APO

        If (ID.EQ.0) then
         JT = 1
         JB = 0
        End if
        If (ID.EQ.N+1) then
         JT = N+1
         JB = N
        END if
        AVNUH = 0.
        DO I=1,M
         AVNUH=AVNUH+(T(I,JB)-T(I,JT))/DELY*2.*DELX*ASPR
        END DO
        RETURN
        END
```

Supplementary File: gridnu.f

```
PARAMETER(M=20,N=10)
```

Input Data File : CONC.DAT

```
0.
2.
1.5
.72
1.e-6
1.e-6
.001
```

VITA

Byungsoo Kim was born in Kunsan, South Korea on September 7, 1970. He graduated from the Science of High School in Kwangju, South Korea in February, 1987. The following March he entered Korea Advanced Institute of Science and technology and in August 1991 received Bachelor of Science degree in mechanical engineering. In August 1992 he entered the University of Tennessee, Knoxville and in December 1994 received a Master of Science degree in mechanical engineering.

He is presently pursuing a Ph. D. degree in mechanical engineering at the Pennsylvania State University, University Park.